





OPEN ACCESS

Original research

A mechanism by which gut microbiota elevates permeability and inflammation in obese/diabetic mice and human gut

Sidharth P Mishra ^{1,2}, Bo Wang,³ Shalini Jain,^{1,2} Jingzhong Ding,⁴ Jared Rejeski,⁴ Cristina M Furdui,⁴ Dalane W Kitzman,^{4,5} Subhash Taraphder,⁶ Christian Brechot,⁷ Ambuj Kumar,⁷ Hariom Yadav ^{1,2}

► Additional supplemental material is published online only. To view, please visit the journal online (<http://dx.doi.org/10.1136/gutjnl-2022-327365>).

For numbered affiliations see end of article.

Correspondence to

Dr Hariom Yadav, Neurosurgery and Brain Repair, University of South Florida College of Medicine, Tampa, FL 33612, USA; hyadav@usf.edu

Received 13 March 2022

Accepted 2 March 2023

Published Online First

22 March 2023

ABSTRACT

Objective Ample evidence exists for the role of abnormal gut microbiota composition and increased gut permeability ('leaky gut') in chronic inflammation that commonly co-occurs in the gut in both obesity and diabetes, yet the detailed mechanisms involved in this process have remained elusive.

Design In this study, we substantiate the causal role of the gut microbiota by use of faecal conditioned media along with faecal microbiota transplantation. Using untargeted and comprehensive approaches, we discovered the mechanism by which the obese microbiota instigates gut permeability, inflammation and abnormalities in glucose metabolism.

Results We demonstrated that the reduced capacity of the microbiota from both obese mice and humans to metabolise ethanolamine results in ethanolamine accumulation in the gut, accounting for induction of intestinal permeability. Elevated ethanolamine increased the expression of microRNA-*miR-101a-3p* by enhancing ARID3a binding on the miR promoter. Increased *miR-101a-3p* decreased the stability of zona occludens-1 (*Zo1*) mRNA, which in turn, weakened intestinal barriers and induced gut permeability, inflammation and abnormalities in glucose metabolism. Importantly, restoring ethanolamine-metabolising activity in gut microbiota using a novel probiotic therapy reduced elevated gut permeability, inflammation and abnormalities in glucose metabolism by correcting the ARID3a/*miR-101a-3p*/*Zo1* axis.

Conclusion Overall, we discovered that the reduced capacity of obese microbiota to metabolise ethanolamine instigates gut permeability, inflammation and glucose metabolic dysfunctions, and restoring ethanolamine-metabolising capacity by a novel probiotic therapy reverses these abnormalities.

Trial registration number NCT02869659 and NCT03269032.

INTRODUCTION

Unfortunately, the prevalence of obesity and type 2 diabetes (T2D) are increasing at alarming rates. Furthermore, the consequences of these diseases are life-threatening end-organ dysfunction; yet no safe, affordable and sustainable prevention and/or treatment is available due to a lack of understanding of

WHAT IS ALREADY KNOWN ON THIS TOPIC

- ⇒ Microbiota abnormalities contribute to obesity and type 2 diabetes (T2D) by triggering metabolic dysfunctions.
- ⇒ Obese gut microbiota instigates intestinal permeability and inflammation, contributing to abnormalities in glucose metabolism in patients with obesity, but detailed mechanisms remain largely unknown.
- ⇒ Specific probiotic therapies may reduce gut permeability and inflammation in obesity and T2D, but most of them lack mechanisms of action.

WHAT THIS STUDY ADDS

- ⇒ Discovered that microbiota of both obese humans and mice diminished ethanolamine-metabolising capacity, which led to increased accumulation of ethanolamine in the gut.
- ⇒ Elevated ethanolamine triggered intestinal permeability by activating *miR-101a-3p* expression via enhancing transcription factor-ARID3a binding on miR promoter.
- ⇒ Ethanolamine-induced *miR-101a-3p* reduced *Zo1* mRNA stability causing reduced *Zo1* formation and weakening intestinal barriers, which in turn caused increased gut permeability, thus inflammation and dysfunction in glucose metabolism.
- ⇒ Meat-supplemented diet promoted ethanolamine accumulation by reducing microbiota's ethanolamine-metabolising capacity.
- ⇒ Restoring ethanolamine-metabolising function of gut microbiota using a human-origin probiotic therapy reversed elevated gut permeability, inflammation and dysfunction of glucose metabolism.

the underlying pathology and mechanisms of risk mitigation efforts.^{1,2} Low-grade chronic inflammation is a key suspect because it is an important driver of obesity-mediated development of dysfunctions in glucose metabolism and T2D. However, its precise aetiology remains elusive. Substantial evidence now exists for elevated gut permeability ('leaky gut')



► <http://dx.doi.org/10.1136/gutjnl-2023-329815>



© Author(s) (or their employer(s)) 2023. Re-use permitted under CC BY-NC. No commercial re-use. See rights and permissions. Published by BMJ.

To cite: Mishra SP, Wang B, Jain S, et al. *Gut* 2023;**72**:1848–1865.

HOW THIS STUDY MIGHT AFFECT RESEARCH, PRACTICE OR POLICY

⇒ The results of these studies not only improve our understanding of the mechanism by which gut microbiota contributes to elevating gut permeability, inflammation and glucose metabolic dysfunction, but they also suggest the future research in order to refine our understanding of mechanism of ARID3a/miR-101a-3p/Zo1 axis in gut permeability, inflammation and metabolic dysfunction. They also indicate the translational potential of ethanolamine-metabolising probiotic therapy to mitigate the risk of T2D in obese patients by ameliorating gut permeability and inflammation. These results may also be beneficial for practitioners and policy makers to make better decisions on dietary guidelines.

being an important and understudied source of systemic inflammation.³ Indeed, elevated gut permeability allows the non-specific transfer of proinflammatory antigens, metabolites and microbes from the gut lumen to intestinal mucosa and the bloodstream, which, in turn, stimulates an inflammatory response through local and systemic immune cells.^{4–7} However, we do not fully understand the mechanistic origins of elevated gut permeability, and thus prevention and treatments are lacking. In the last two decades, a mounting body of evidence suggests that the gut of the obese patients can harbour significantly different microbiota than are found in non-obese individuals. In particular faecal microbiota transplantation (FMT) of obese microbiota increases (causal) the risk of T2D, along with an increase in gut permeability and inflammation in recipient mice.⁸ However, we still do not understand how an obese microbiota instigates gut permeability, and consequently increases inflammation and dysfunctional glucose metabolism as seen in T2D.

Gut permeability is limited by abundant and healthy tight junction complexes that connect epithelial cells, sustaining normal intestinal integrity.⁹ Tight junction complexes are made from zona occludens-1 (*Zo1*) or occludins and claudins. This evidence comes from independent studies showing that cells lacking *Zo1* show higher permeability and flux of large (40 kDa) solutes,^{10,11} indicating that the *Zo1* is essential to maintain normal epithelial barrier functions and permeability. Conversely, the expression of *Zo1* in the intestine is significantly reduced in the gut of obese and T2D, and associated with elevated gut permeability, inflammation and abnormal gut microbiota¹²; however, the mechanisms which lead to a decrease in *Zo1* expression remain largely unknown. Emerging evidence indicates that the metabolites produced by gut microbiota influence the expression of *Zo1* and thus gut permeability.^{9,13} Beneficial microbial metabolites like short-chain fatty acids, indole derivatives, bile acid derivatives and conjugated fatty acids promote expression of *Zo1* and reduce gut permeability^{14–17}; conversely, there is an incomplete understanding of whether, how and which microbiota metabolites may reduce *Zo1* expression and instigate gut permeability. Furthermore, we also do not understand many details of the mechanisms by which microbial metabolite productions are influenced, nor do we understand the mechanism(s) by which they impact *Zo1* expression, and thus perturb the gut barriers.

In this context, we now know that the host–microbe interactions induce epigenetic changes in intestinal cells, which play a crucial role in maintaining intestinal barrier functions and host health.¹⁸ In particular, host-produced micro(mi)-RNAs shape the gut microbiota while gut microbiota and its metabolites influence

the expression of miRNAs in gut epithelial cells; this mechanism involves continuous and bidirectional interactions between the gut microbiota and the host through miRNAs.^{19,20} The miRNAs are small endogenous non-coding, 18–25 nucleotides RNAs that control gene expression by binding to specific sequences on the 3'-untranslated region (3'-UTR) of the target mRNA via base complementarity, thereby inducing translational repression, degradation or both, of target mRNA.²¹ We do not understand, however, which and how microbial metabolites regulate those miRNAs involved in driving intestinal tight junctions like *Zo1* and gut permeability.

This study demonstrates a novel mechanism that accounts for the gut microbiota's impact on elevated gut permeability and inflammation in obese models and human subjects. We discovered that the obese gut yields increased ethanolamine due to suppressed ethanolamine-metabolising bacteria. Moreover, we have deciphered the detailed mechanism by which ethanolamine increased ARID3a, miR101a-3p, which in turn reduced *Zo1* expression, thereby elevating gut permeability, inflammation and dysfunction in glucose metabolism. Finally, we provide solid evidence for the potential to intervene in this chain of events by modelling the gut microbiota through probiotics.

RESULTS**Obese microbiota instigates leakiness in gut by reducing tight junctions, which in turn triggers inflammation and metabolic dysfunctions**

Obese FMTs induce gut permeability, inflammation and glucose metabolic dysfunctions in mice

Despite knowing that the obese gut harbours an abnormal microbiota along with increased gut permeability, inflammation and impaired glucose metabolism^{8,22} direct evidence as to whether and how gut microbiota induces gut permeability remains elusive. Interestingly, we showed that both FMT and cecal microbiota transplantation (CMT) of obese (both db/db (leptin receptor knock-out obese and diabetic), and diet-induced obese (DIO) mice) significantly increased gut permeability (measured by increased diffusion of fluorescein isothiocyanate (FITC)-dextran (4 and 40 kDa as well as FITC-lipopolysaccharide (LPS) conjugate) from gut to blood (figure 1A; online supplemental figure 1a,b). In addition, circulating levels of (LPS/Endotoxin), LPS-binding protein (LBP) and soluble CD14 (sCD14) and microbial 16S rDNA in serum were increased in FMT and CMT recipient mice (figure 1B–E; online supplemental figure 1c,d). These changes were linked with increased expression of inflammatory markers (interleukin-1beta (*Il1β*), *Il6* and tumor necrosis factor-alpha (*Tnfa*)) in the gut of recipient mice (figure 1F). Further, the HEK-blue-TLR4 cells treated with serum of db/db and DIO-FMT recipients (containing elevated LPS/endotoxin) and showed significantly higher TLR4 activity compared with lean control FMT and CMT recipient serum treated cells (figure 1G, online supplemental figure 1e); suggesting that the LPS leaked from gut activates inflammatory receptor like toll-like receptor 4 (TLR4) and drives metabolic endotoxaemia. Interestingly, an increase in markers of elevated gut permeability and inflammation in recipient mice were similar to the donor mice (online supplemental figure 2a–d; and published by us elsewhere²³). Notably, both obese FMT and CMT also significantly increased dysfunctions in metabolic health such as increases in body weight gain, food intake, fasting blood glucose, impaired meal and insulin tolerance, elevated levels of fasting insulin and HOMA-IR (Homeostatic Model Assessment for Insulin Resistance) in recipient mice (figure 1H–L; online supplemental figure

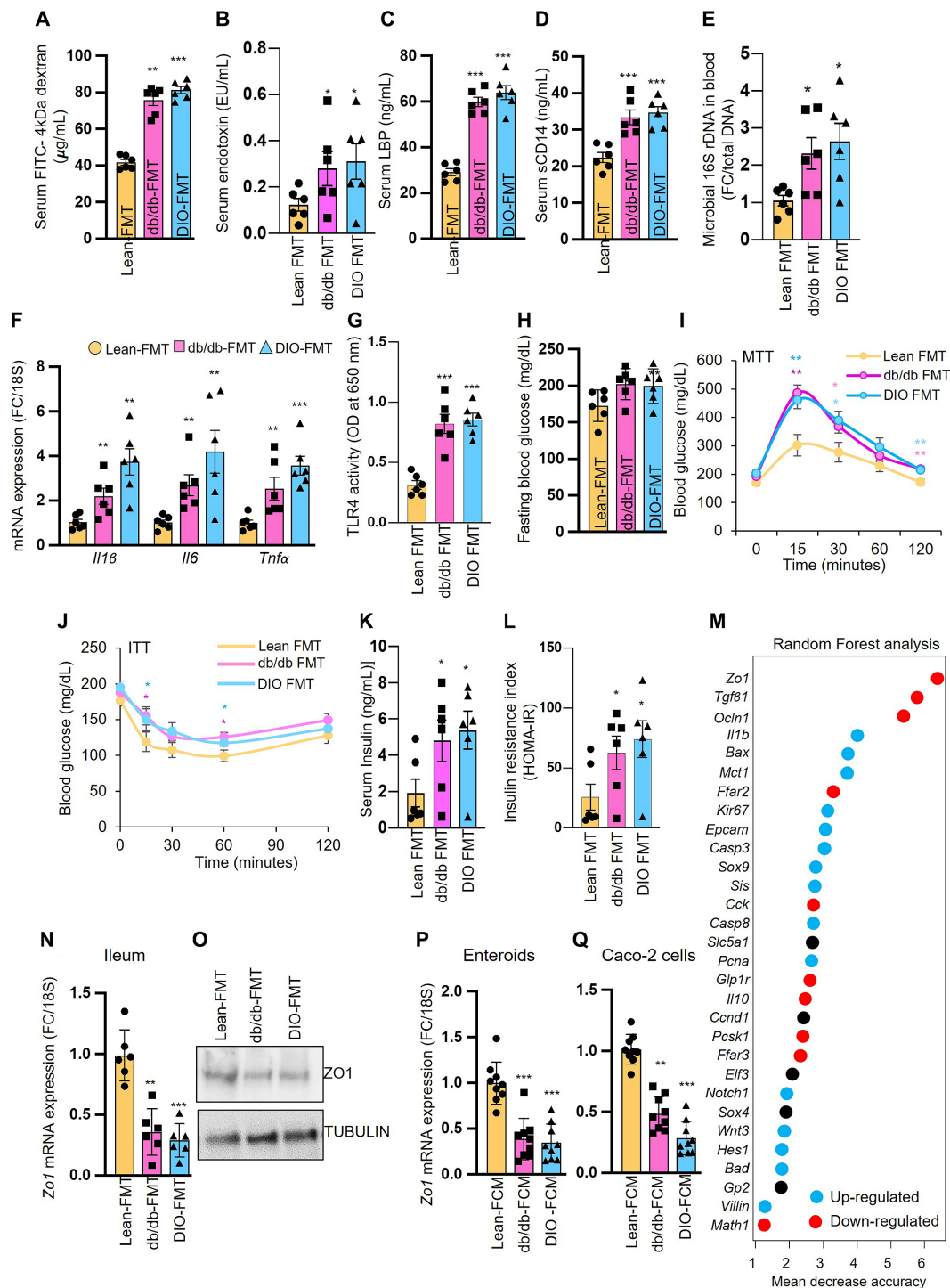


Figure 1 Obese microbiota is causal to instigate elevated gut permeability, inflammation and metabolic dysregulation. (A, B) Mice receiving FMT from both db/db and DIO mice showed significant increase in FITC 4kDa-dextran (A), endotoxin (LPS) (B) leakage from gut to blood compared with their lean control FMT recipient mice. (C–F) In addition, these mice also show significantly increased levels of systemic markers of elevated gut permeability (LBP (C) and sCD14 (D)), as well as microbial 16S rDNA (fold change (FC)) in serum (E) mRNA expression of inflammatory markers (*Il1β*, *Il6* and *Tnfa*) (F) compared with their controls. (G) The TLR4 activity (absorbance at 650 nm) was significantly increased in HEK-Blue mTLR4 cells treated with serum of db/db and DIO FMT recipient mice compared with the lean FMT controls. (H–L) Obese FMTs also increased fasting hyperglycaemia (H) along with impaired meal tolerance test (MTT) (I), insulin tolerance test (ITT) (J), increased serum insulin (K) and insulin resistance index (HOMA-IR) (L). (M) Random forest analysis of gene expression data revealed that obese FMTs and FCMs treatment dramatically reduced *Zo1* expression in intestine and enteroids, respectively, compared with their lean FMTs/FCMs treated controls. (N–Q) Further, the expression of *Zo1* mRNA (N–P) and protein (O) in the ileum (N, O), enteroids (P) and Caco-2 cells (Q) of obese FMTs recipient mice and FCMs treated enteroids and Caco-2 cells, respectively, compared with their controls. Values presented are mean (n=5–8 mice per group) and error bars as the SEM. Enteroids and Caco-2 cell culture experiments were performed in triplicates and repeated 2–3 times. *p<0.05, **p<0.01, ***p<0.001 are statistically significant analysed by the t-test and/or ANOVA. ANOVA, analysis of variance; DIO, diet-induced obese; FCM, faecal conditioned media; FMT, faecal microbiota transplantation; HOMA-IR, Homeostatic Model Assessment for Insulin Resistance; LBS, LPS-binding protein; LPS, lipopolysaccharide.

3a–k). Collectively, these results indicate that transplanting obese microbiota promoted gut permeability, inflammation and metabolic dysfunctions in recipient mice.

Faecal conditioned media recapitulates FMT in an intestinal monolayer cell model

Treatment of faecal conditioned media (FCM) prepared from faeces of db/db and DIO mice significantly reduced the transepithelial electrical resistance (TEER) and increased diffusion of FITC-dextran (4 and 40 kDa, and LPS) through Caco-2 cell monolayers compared with control lean mice FCM (online supplemental figure 4a–d). These results indicate that FCM treatments exhibit similar results to those of obese FMTs/CMTs in the intestinal monolayer cell model, indicating FCM recapitulates FMT effects on intestinal barriers.

Both obese FMT and FCM reduce the expression of tight junctions in mouse intestines, cells and enteroid models

To decipher the mechanism(s) by which obese microbiota elevated gut permeability and inflammation, a gene array was used to determine key genes ($n=53$; online supplemental table 1) of intestinal epithelia and inflammatory markers. Our unbiased random forest analysis (RFA) revealed that the zona occludens-1 (*Zo1*) expression was most significantly reduced in the intestine of FMT recipients and intestinal organoids (enteroids) treated with FCM of obese faeces compared with controls (figure 1M; online supplemental table 2). Further, differential gene expression analyses (volcano graphs) also showed that the *Zo1* expressions were significantly decreased in the intestine and enteroids treated with obese FMTs and FCMs, respectively (online supplemental figure 4e–g), a conclusion which was further confirmed to be significantly by finding decreased expression of *Zo1* in the intestine, enteroids and Caco-2 cells treated with obese FMT and FCM, respectively (figure 1N–Q). Overall, these results demonstrated that the obese microbiota instigates elevation in gut permeability by reducing the expression of *Zo1*, thus weakening intestinal barrier functions.

The obese gut has elevated ethanolamine, which induces gut permeability, inflammation and impaired glucose metabolism by dampening tight junction barriers

Microbiota produce a wide range of metabolites that impact intestinal epithelial and systemic cellular functions; but which microbial metabolites decrease *Zo1* expression in the obese intestine are not known. Our unbiased, untargeted global metabolomics and principal component analyses in faeces revealed that obese (both db/db and DIO) gut harboured a very different metabolite signature than was found in controls (NC fed and low-fat diet, LFD-fed, respectively) (figure 2A). Further, unbiased random forest and differential abundance analyses show that six metabolites—ethanolamine, valine, isoleucine, cholate, anserine and leucine—were highest in the gut of DIO and db/db mice compared with the age-matched, sex-matched and diet-matched controls (figure 2B; online supplemental figure 5a,b). Interestingly, among them, ethanolamine showed the greatest reduction in the expression of *Zo1* in the enteroids and Caco-2 cell monolayers (figure 2C,D), and significantly increased in the permeability of FITC-dextran/LPS and epithelial integrity (TEER) in Caco-2 cell monolayers (figure 2E,F; online supplemental figure 6a,b). Additionally, the ethanolamine treatment significantly increased FITC-dextran permeability with dampened TEER in *Zo1* overexpressing (lentivirus mediated) Caco2 cells (online supplemental figure 7a–d), thus indicating

that the ethanolamine gut permeability promoting effects were solely mediated by reducing *Zo1* barriers. Furthermore, 7-day ethanolamine treatment to mice also significantly reduced the expression of *Zo1*, along with increased intestinal permeability, endotoxaemia, inflammation and metabolic dysfunctions, that is, impaired meal tolerance and insulin tolerance along with hyperinsulinaemia (figure 2G–P, online supplemental figure 8a–c). These results indicate that the obese gut accumulated higher ethanolamine which in turn reduced the expression of *Zo1* to weaken intestinal barrier functions, causing elevated gut permeability, inflammation and dysfunction in glucose metabolism.

Ethanolamine was increased in the obese gut due to decreased ethanolamine-metabolising bacteria

Our studies show that increased ethanolamine accumulation in obese gut promotes leakiness in gut by reducing *Zo1*; but how remains unknown. We observed that the abundance of bacteria expressing ethanolamine-using ('metabolising') (*Eut*) operon genes (ie, *eutA*, *eutB*, *eutC*, *eutD*, *eutP*, *eutQ*, *eutS* and *eutT*) was significantly lower in the stools of obese (both db/db and DIO) mice compared with their controls (figure 3A), and was negatively correlated with ethanolamine and markers of elevated gut permeability (serum FITC, LBP and sCD14 levels) and inflammation (*Il1 β* , *Il6* and *Tnfa*), and was positively correlated with *Zo1* mRNA levels (figure 3B, online supplemental table 3), suggesting that there was a reduced abundance of ethanolamine-metabolising bacteria, leading to higher ethanolamine accumulation.

To establish clinical relevance of our findings, we showed that the metabolomic signatures in stools of obese humans differed substantially from lean controls (figure 3C, online supplemental table 4 and online supplemental figure 9a); and, most importantly, the abundance of ethanolamine was highest in the gut of obese subjects compared with lean ones (figure 3D, online supplemental figure 9b). Increased faecal ethanolamine levels were positively correlated with body mass index (BMI) of human subjects (figure 3E). In addition, *Eut* operon expression was also lower in the stools of obese subjects than in normal weight controls (figure 3F), which was negatively correlated with BMI (figure 3G, online supplemental figure 9c). These results suggested that the higher ethanolamine accumulation in obese gut due to reduced ethanolamine-metabolising bacteria were similar in mice and humans and indicate their translational importance to be implemented in the clinic.

Obese microbiota and ethanolamine promote gut permeability by increasing *miR-101a-3p* expression

To further determine how elevated ethanolamine reduced *Zo1* thereby elevating gut permeability, we tested a hypothesis that obese microbiota and its metabolite—ethanolamine modulate epigenetic factors like miRNAs in intestinal cells to reduce *Zo1* expression and induce gut permeability. Our unbiased, global miRNA expression analyses revealed that the enteroids treated with db/db and DIO FCMs show significantly distinct miRNA signatures compared with their controls (figure 4A). Further, random forest analyses revealed that the expression of *miR-101a-3p* was highest in enteroids treated with obese FCMs compared with controls (figure 4B, online supplemental figure 10a,b; online supplemental table 5), a result that we later confirmed by real-time PCR analyses in FCM treated enteroids and Caco-2 cells (figure 4C,D). The expression of *miR-101a-3p* was also significantly higher in ileum and colon of faecal donor db/db and DIO and their FMT recipient mice, compared with

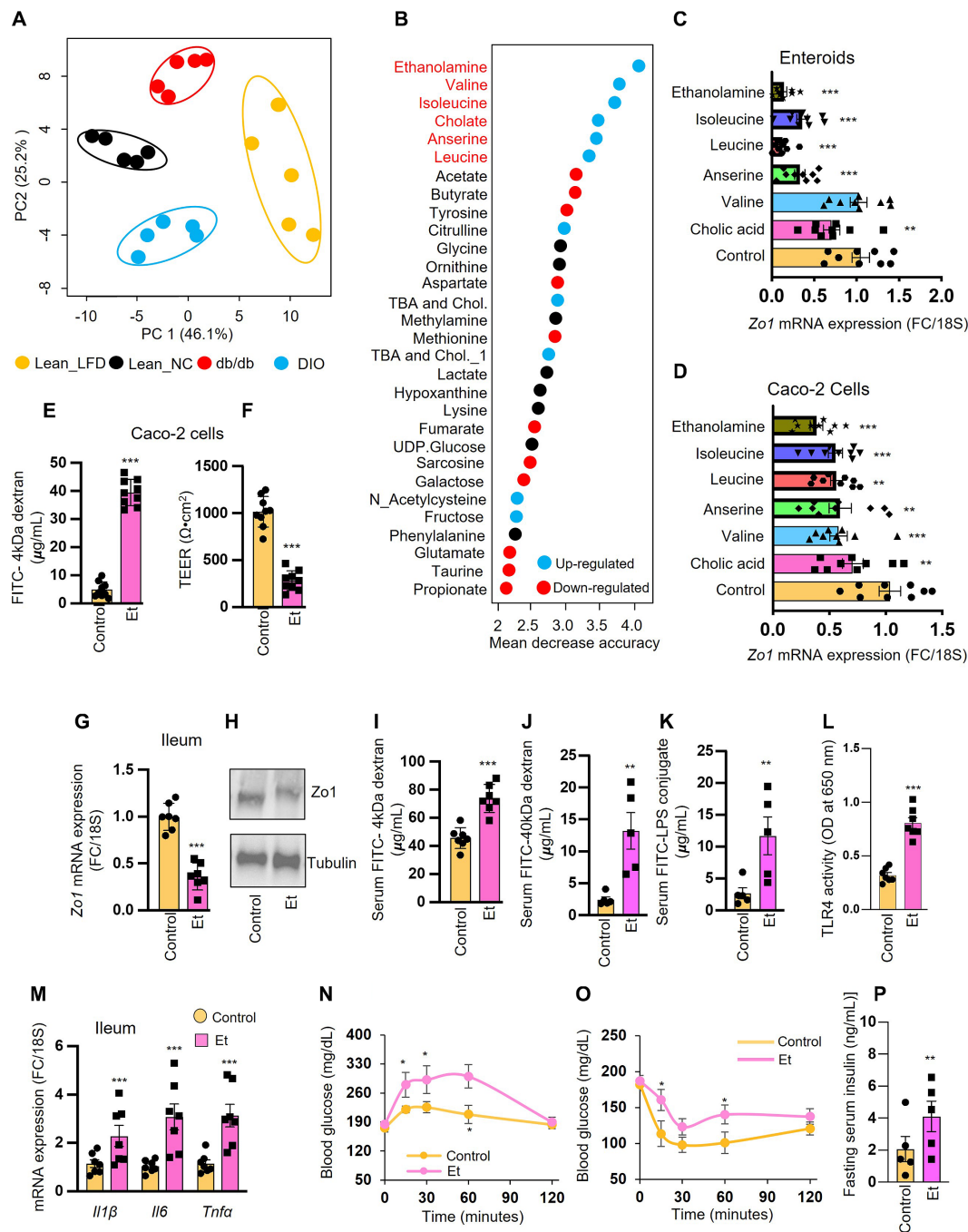


Figure 2 Obese gut accumulates higher ethanolamine, which in turn instigates gut permeability, inflammation and impaired glucose metabolism. (A) Principal component analysis (PCA) of metabolomics data shows that metabolites in the faeces of obese (db/db (red) and DIO (blue)) mice compared with their controls (B6 NC (black) and B6 LFD (gold accent)) mice are significantly distinct. (B) Random forest analysis shows that ethanolamine abundance was significantly higher in the obese gut compared with their controls. (C, D) Ethanolamine most dramatically reduced the expression of *Zo1* mRNA in the enteroids (C) and Caco-2 cells (D) among the top 6 selected metabolites (red in b panel) such as isoleucine, leucine, anserine, valine and cholic acid. (E, F) Further, ethanolamine (Et) treatment also dramatically increased the permeability of FITC-dextran (E) and reduced TEER (F) in the monolayers of Caco-2 cells. (G–L) Oral administration of ethanolamine (Et) (1 g/kg body weight for 7 days) in mice significantly reduced expression of *Zo1* (mRNA (g) and protein (h)) in ileum along with increased gut permeability (FITC (4 and 40 kDa) and LPS-conjugate-dextran assay (I–K)), along with increased TLR4 activity in mouse serum treated HEK-Blue mTLR4 cells (L). (M–P) It also increased the inflammation (*Il1β*, *Il6* and *Tnfa*) (M) in the intestine (ileum) and impaired insulin MTT (N) and ITT (O) with increased fasting blood glucose (P) compared with their controls. Values presented are mean of n=5–8 mice and n=2–3 repeated triplicate enteroids and Caco-2 cell culture experiments in each group, and error bars are SEM. *p<0.05, **p<0.01, ***p<0.001 are statistically significant analysed by the t-test and/or ANOVA. ANOVA, analysis of variance; DIO, diet-induced obese; ITT, insulin tolerance test; LFD, low-fat diet; LPS, lipopolysaccharide; MTT, meal tolerance test; TEER, transepithelial electrical resistance.

the respective controls (figure 4E–H). Intriguingly, ethanolamine treatment also increased the expression of miR-101a-3p expression in mouse intestine as well as in enteroids and Caco-2

cell monolayers (figure 4I, J; online supplemental figure 11a, b), suggesting that the obese microbiota and ethanolamine induced the expression of miR-101a-3p in gut epithelial cells. Further,

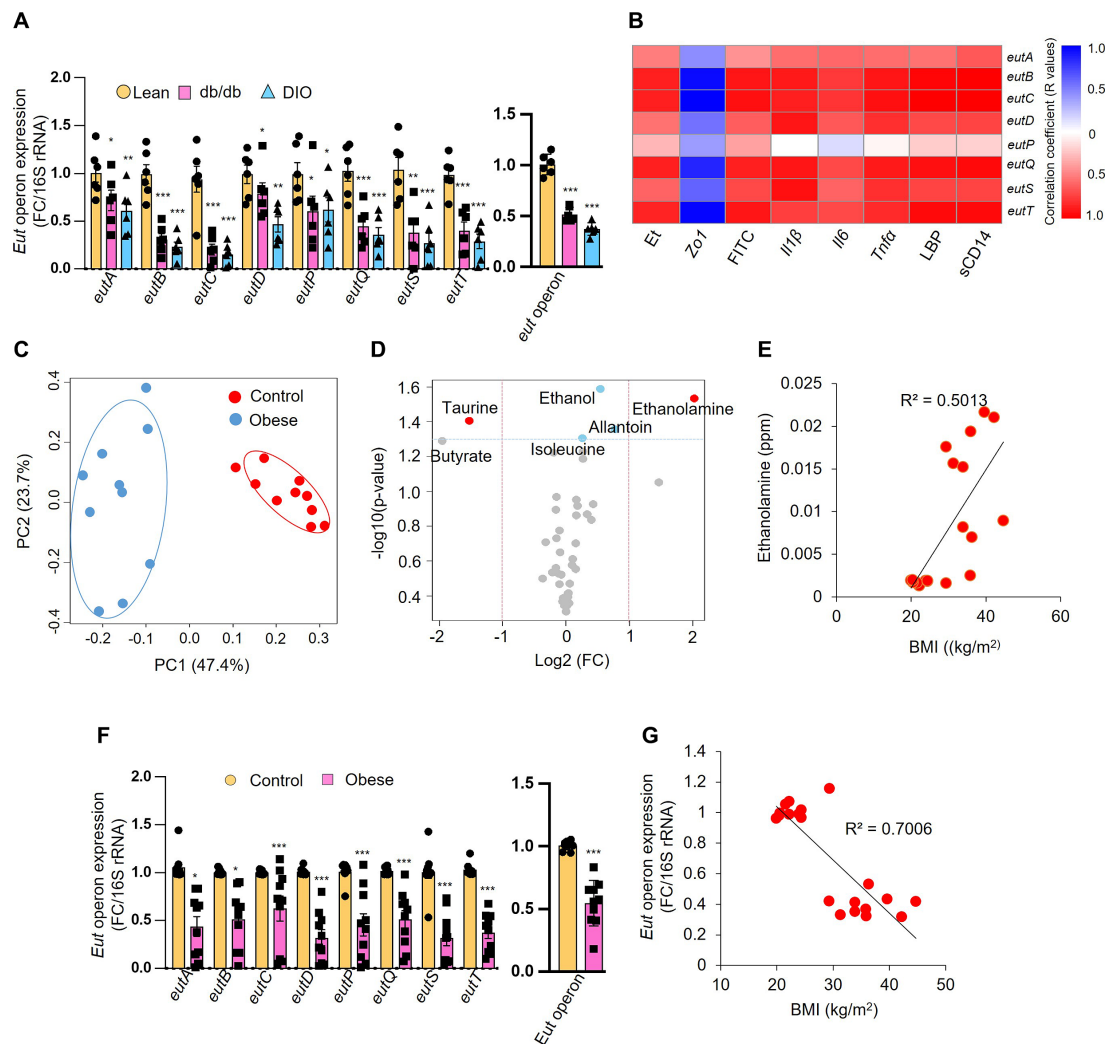


Figure 3 Ethanolamine abundance in the gut of obese mice and humans increases due to its undermetabolisation by microbiota. (A) The expression of ethanolamine utilising (*Eut*) operon genes (*eutA*, *eutB*, *eutC*, *eutD*, *eutP*, *eutQ*, *eutS*, *eutT* and aggregate of all genes as *Eut* operon) was significantly decreased in the faeces of db/db and DIO mice compared with lean controls. (B) Interestingly, the reduced expression of these genes was negatively correlated with ethanolamine (Et) abundance, as well as markers of elevated gut permeability (FITC-dextran leakiness, LBP and sCD14) and inflammatory markers (*Il1β*, *Il6* and *Tnfα*) and positively correlated with the expression of *Zo1* in the mouse intestine. (C, D) Interestingly, PCA analyses (C) show that metabolite signature was significantly different in 10 normal weight (control) compared with 10 obese subjects, and differential abundance analyses in volcano graph (D) show that ethanolamine abundance was significantly higher in the gut of obese compared with control subjects. (E) Increased ethanolamine abundance shows a strong positive correlation. (F,G) Notably, the expression of ethanolamine utilising operon genes (F) was significantly reduced in obese stools compared with their controls and showed a negative correlation with BMI (G). Values presented are mean of n=5–8 mice and n=10 lean and n=10 obese subjects in each group, and error bars are SEM. PCA (C), volcano (D) and correlation analyses (E,G) show individual sample values. *p<0.05, **p<0.01, ***p<0.001 are statistically significant analysed by the t-test and/or ANOVA. ANOVA, analysis of variance; BMI, body mass index; LBP, LPS-binding protein; LPS, lipopolysaccharide; PCA, principal component analysis.

the enema of miR-101a-3p expressing lentivirus in mice also significantly increased gut permeability, endotoxaemia and inflammation along with reduced expression of *Zo1* in the intestine compared with scrambled lentivirus treated controls (figure 4K–Q, online supplemental figure 11c). Overall, these results demonstrated that the elevated ethanolamine in the gut promoted expression of miR-101a-3p in gut epithelial cells, which induced gut permeability.

Ethanolamine elevates *miR-101a-3p* expression by activating its promoter activity

Ethanolamine treatment significantly increased the promoter luciferase activity of miR-101a-3p in Caco-2 cells (figure 5A), suggesting that ethanolamine increased miR-101a-3p by activating

its promoter. To further determine which DNA region(s) of miR-101a-3p promoter (2000 bp long)²⁴ contributes in ethanolamine-induced activation, we show that cells transfected with a vector containing a sequence of –1 to –1000 bp region exhibit the highest luciferase activity on ethanolamine treatment, but moderate and no effects in cells transfected with –1 to –1500 bp and –1 to 500 bp fragments, respectively (figure 5B). These results indicated that the promoter region between –1 and –500 bp does not participate in ethanolamine mediated activation of miR-101a-3p promoter while fragment –1 to –1000 bp and –1 to –1500 bp show the highest to moderate activation, which might be because both the fragments contain –500 to –1000 bp fragment. Thus, –500 to –1000 bp fragment is the key region involved in ethanolamine-induced activation of this promoter.

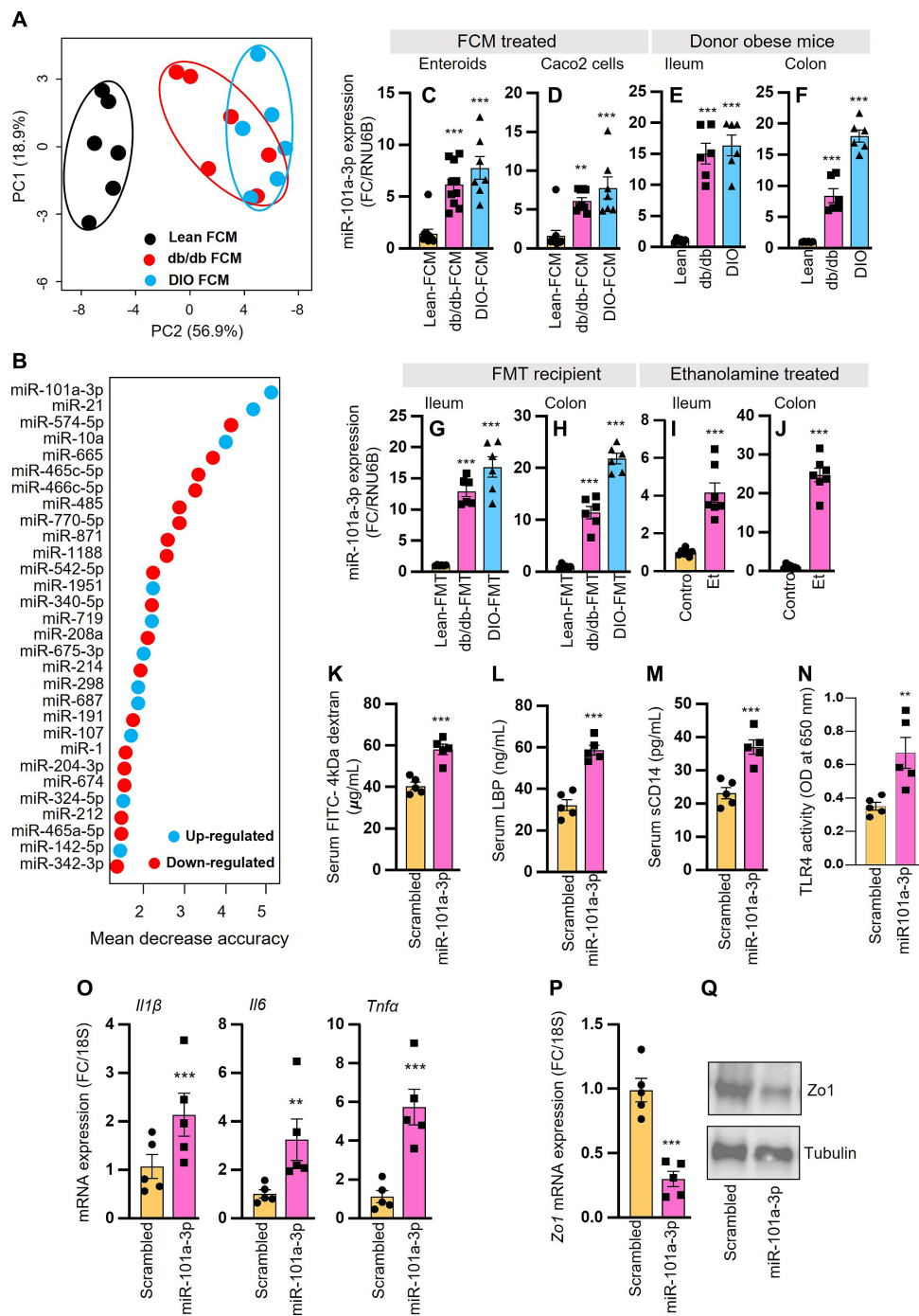


Figure 4 Ethanolamine and obese microbiota enhance the expression of *miR-101a-3p*, which in turn induce gut permeability by reducing ZO-1 expression. (A) PCA graph of global miRNA profiles from enteroids treated with FCMs of db/db and DIO mice show significantly distinct miRNA expression profiles compared with lean controls. (B–D) Random forest analyses of miRNA data revealed that *miR-101a-3p* expression was significantly increased in enteroids treated with FCMs of db/db and DIO mice compared with lean controls (B), which was verified by real-time qPCR analyses in enteroids (C) and Caco-2 cells (D). (E, F) The expression of *miR-101a-3p* expression was also significantly higher in both ileum (E) and colon (F) of donor db/db and DIO mice. (G–J) The expression of *miR-101a-3p* was also increased in the ileum (G, I) and colon (H, J) of FMT recipients (G, H) and ethanolamine (Et) treated mice (I, J) compared with their controls. (K–N) Intriguingly, enema of lentivirus expressing *miR-101a-3p* mimetic significantly increased gut permeability (FITC-dextran (K), LBP (L) and sCD14 (M) in serum), and that serum increases TLR4 activity in HEK-Blue mTLR4 cells (N) which corresponds to increased inflammation (*Il1 β* , *Il6* and *Tnfa*) (O) and reduced *Zo1* mRNA (P) and protein (Q) in the mice gut compared with their scrambled miR lentivirus infected mice. Values presented are the mean of $n=5-8$ mice in each group, and error bars are the SEM. PCA (A) and random forest analyses (B) show individual sample values. * $p<0.05$, ** $p<0.01$, *** $p<0.001$ are statistically significant analysed by the t-test and/or ANOVA. ANOVA, analysis of variance; DIO, diet-induced obese; FCM, faecal conditioned media; FMT, faecal microbiota transplantation; PCA, principal component analysis.

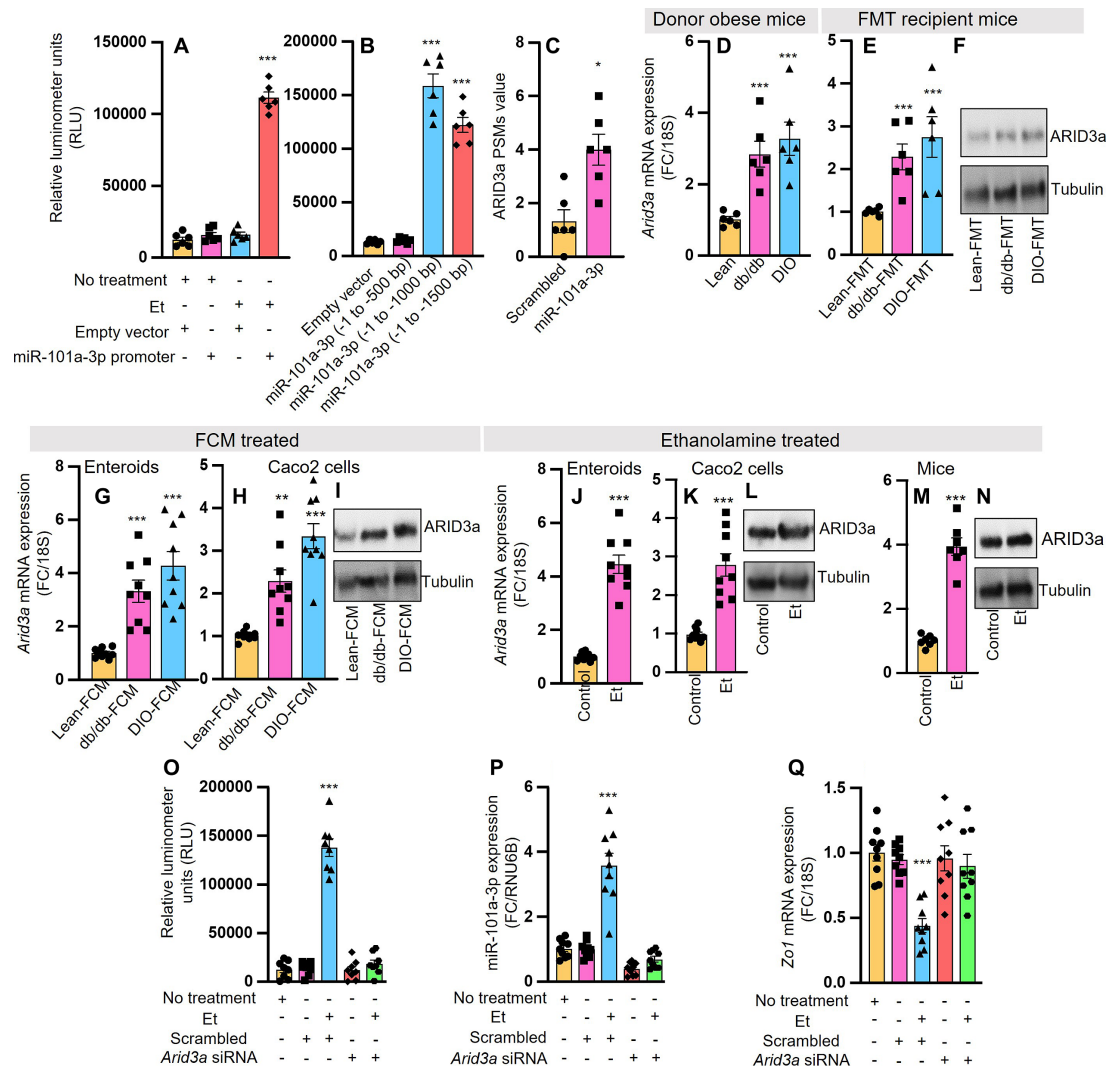


Figure 5 Ethanolamine increases *miR-101a-3p* expression by increasing its promoter activity by enhancing transcription factor ARID3a binding on it. (A) Ethanolamine increases *miR-101a-3p* promoter depicted by luciferase assay in Caco-2 cells transfected with a vector carrying *miR-101a-3p* promoter (-1 to -2000 bp of transcript start site (TSS)) compared with empty vector-transfected cells. (B) Further, ethanolamine treatment significantly increased *miR-101a-3p* promoter activity in the Caco-2 cells transfected with vectors carrying -1 to -1000 bp and -1 to 1500 bp fragments, while no change was observed in cells transfected with a vector carrying -1 to 500 bp and empty vector. (C) Unbiased and untargeted ChIP-pull-down analyses revealed that a transcription factor-ARID3a was the highest protein pulled out with -500-1000 bp fragment compared with a scrambled nucleotide DNA sequence. (D, E) Interestingly, expression of *Arid3a* mRNA (D, E) and protein (F) was found significantly higher in the gut of donor db/db and DIO mice (D) as well as in FMT recipients (E, F) (G-I) In addition, obese/T2D FCMs (G-I) and ethanolamine (J-N) treatments significantly increased the expression of *Arid3a* in the enteroids (G, J), Caco-2 cells (H, I, K, L) and mouse intestine (M, N) compared with controls. (O-Q) Notably, ethanolamine-mediated activation of *miR-101a-3p* promoter activity (O), *miR-101a-3p* expression (P), and suppression in *Zo1* expression (Q) were abolished in ARID3a siRNA transfected Caco-2 cells compared with scrambled siRNA transfected cells. Values presented are the mean of n=5-8 mice, n=2-3 repeated triplicate enteroids and Caco-2 culture experiments in each group; error bars are the SEM. *p<0.05, **p<0.01, ***p<0.001 are statistically significant analysed by independent t-test and/or ANOVA. ANOVA, analysis of variance; FCM, faecal conditioned media; FMT, faecal microbiota transplantation; T2D, type 2 diabetes.

Ethanolamine activates *miR-101a-3p* promoter by enhancing binding of a transcription factor-ARID3a on *miR* promoter

To further discover how ethanolamine induced *miR-101a-3p* promoter, we performed an unbiased promoter-protein binding pull-down assay, using -500 to -1000 bp fragment of *miR-101a-3p* promoter and non-targeted proteomic analyses and found that a transcription factor—ARID3a—was especially abundant in *miR-101a-3p* promoter-transfected pull-down samples compared with scrambled promoter transfected controls (figure 5C and online supplemental figure 12a-c). Further, our in-silico analyses on search engines such as oPOSSOM V3

and ConTra V3 found that ARID3a has a predictive binding sequence on the *miR-101a-3p* promoter (online supplemental figure 13a,b). Interestingly, ARID3a expression was significantly higher in the intestines of db/db and DIO, their FMT recipients, ethanolamine-treated mice as well as in enteroids and Caco-2 cell monolayers treated with db/db and DIO FCMs and/or ethanolamine compared with their corresponding controls (figure 5D-N, online supplemental figure 14a-d). Intriguingly, ARID3a siRNA transfected Caco-2 cells show no increase in the *miR-101a-3p* promoter luciferase activity, *miR-101a-3p* expression and *Zo1* mRNA on ethanolamine treatment compared with

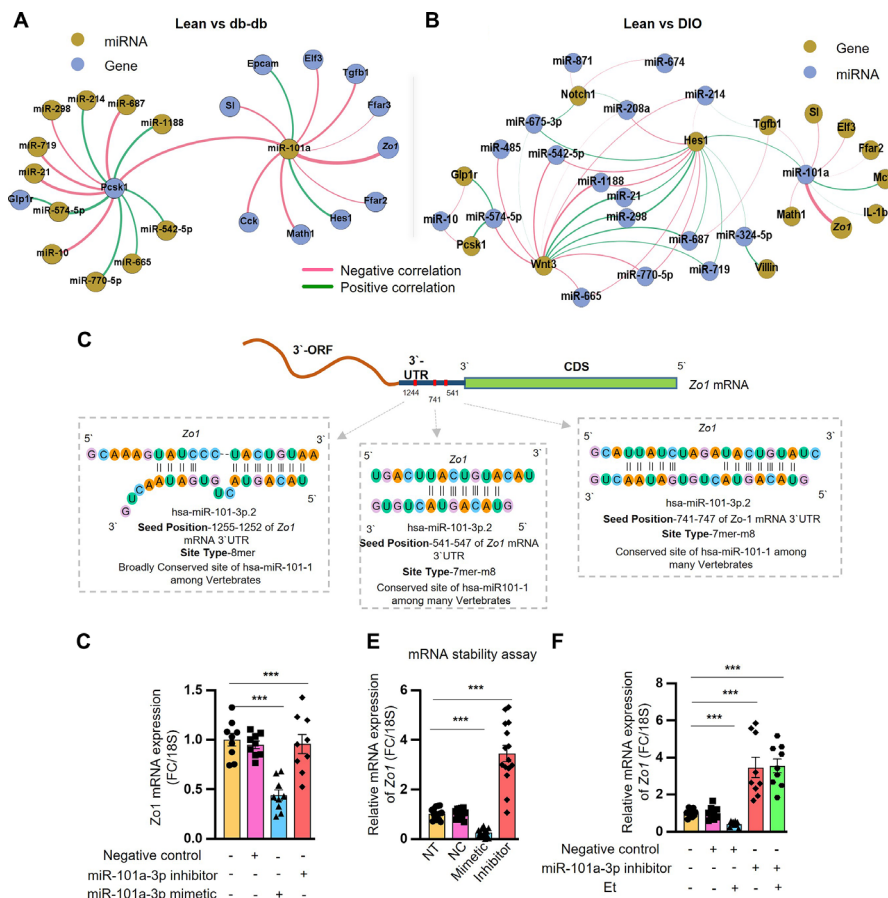


Figure 6 Ethanolamine induces miR-101a-3p, which in turn reduces *Zo1* expression by decreasing its mRNA stability. (A, B) Correlation networking analyses of miRNA and intestinal cell-specific gene expression profiles in intestines from obese (db/db (A) and DIO (B)) FMT recipient mice and enteroids treated with obese FCMs show that miR-101a-3p and *Zo1* show the highest negative correlation. (C) Representation of three miR-101a-3p binding sites on human *Zo1* mRNA 3'UTR sequence (seed positions). (D) miR-101a-3p mimetic (Agomir) significantly reduced expression of *Zo1* mRNA while miR-101a-3p inhibitor oligonucleotide reversed it. (E) The miR-101a-3p mimetic significantly reduced the stability of *Zo1* mRNA, while the miR-101a-3p inhibitor reversed it. (F) The miR-101a-3p inhibitor abolished the ethanolamine effects of reducing *Zo1* mRNA expression. Values presented are the mean of $n=2-3$ repeated triplicate of Caco-2 culture experiments in each group, and error bars are the SEM. * $p<0.05$, ** $p<0.01$, *** $p<0.001$ are statistically significant analysed by t-test and/or ANOVA. 3'-UTR, 3'-untranslated region; ANOVA, analysis of variance; FCM, faecal conditioned media; FMT, faecal microbiota transplantation; DIO, diet-induced obese.

scrambled controls (figure 5O–Q), indicating that the ethanolamine effects on miR-101a-3p promoter are mediated through ARID3a binding. Collectively, these results demonstrated that the elevated ethanolamine in the gut activates ARID3a binding on the miR-101a-3p promoter to increase miR-101a-3p expression, which, in turn, reduces *Zo1* expression.

miR-101a-3p reduces *Zo1* expression by decreasing its mRNA stability

Our correlation network analyses, combining miRNA profiles and gene expression data from intestines of FMT recipients, FCM-treated enteroids and Caco-2 cells versus controls revealed the highest negative correlation between miR-101a-3p and *Zo1* (figure 6A,B; online supplemental figure 15a–e; online supplemental table 6a,b), suggesting that increased miR-101a-3p expression is predominantly linked with decreased *Zo1* expression. Notably, miRNA target analyses also revealed that the 3'-UTR of *Zo1* mRNA consisted of three potential miR-101a-3p binding sites (figure 6C), indicating that miR-101a-3p can directly bind to the *Zo1* mRNA to alter its expression. Further, Caco-2 cells transfected with miR-101a-3p-mimetic significantly reduced the mRNA levels of *Zo1* while miR-101a-3p inhibitor

reversed these changes (figure 6D), suggesting that the miR-101a-3p reduced *Zo1* mRNA stability. The overexpression of miR-101a-3p-mimetic in Caco-2 cells remarkably reduced the stability of *Zo1* mRNA while miR-101a-3p inhibitor reversed it (figure 6E,F; online supplemental figure 16a,b). In addition, the effect of ethanolamine in reducing *Zo1* expression disappeared in miR-101a-3p inhibitor-treated cells. These results indicated that the microbiota/ethanolamine-induced miR-101a-3p bound to *Zo1* mRNA and reduced its stability, resulting in diminished *Zo1* expression.

Ethanolamine-metabolising bacteria decrease primarily in the ileum, leading to intestinal leakiness: high fat-supplemented and meat-supplemented diets augment this regional bacterial decline

We then asked whether the decrease in ethanolamine-metabolising bacteria was region-specific or prevalent in whole intestine. We found that the expression of *Eut* operon genes (*eutA*, *eutB*, *eutC*, *eutD*, *eutP*, *eutS*, *eutT*) was the lowest in ileal fluid compared with other intestinal sections, specifically the duodenum, jejunum and colon in mice who received obese

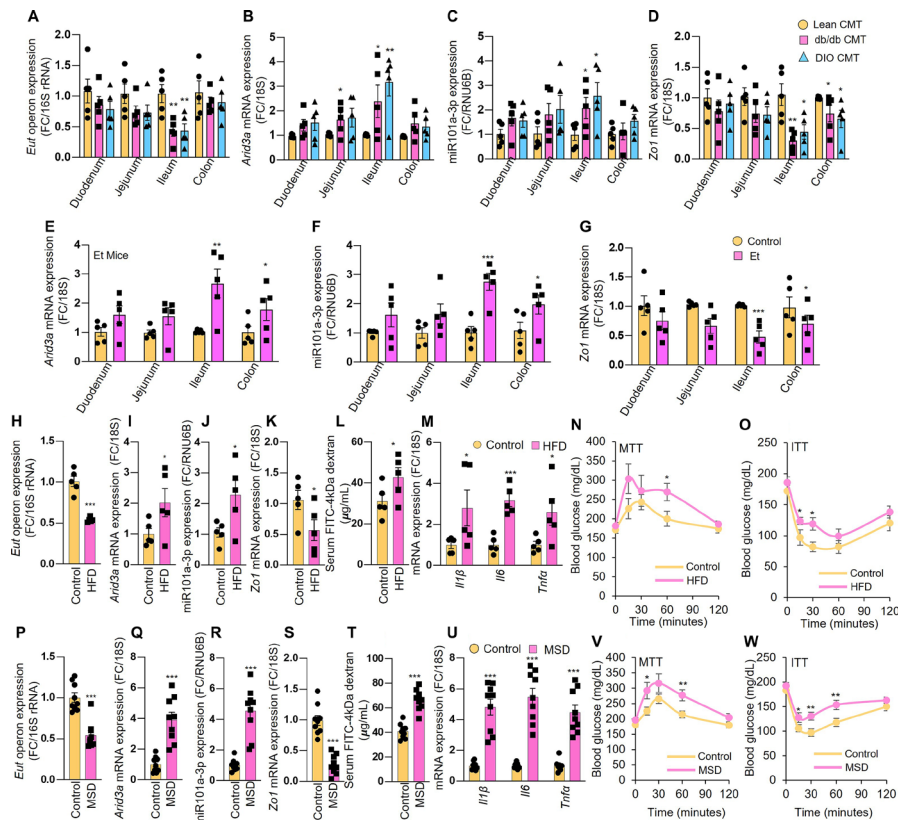


Figure 7 The ileum is primarily deficient in ethanolamine-metabolising bacteria with higher leakiness, and a high-fat diet (HFD) and meat-supplemented diet (MSD) reduce them. (A–D) abundance of *Eut* operon (A) significantly and predominantly reduced in ileum of obese FMT recipient mice compared with other sections like duodenum, jejunum and colon, which were linked with increased expression of *ARID3a* (B), miR101a-3p (C) and reduced *Zo1* (D) mRNA in the ileal section. (E–G) similarly, ethanolamine (et) treatment primarily increased the expression of *ARID3a* (E) and miR101a-3p (F) and reduced *Zo1* (G) mRNA primarily in the ileum compared with other sections like duodenum, jejunum and colon. (H–W) The feeding of HFD (H–O) and MSD (P–W) similarly and significantly reduced the abundance of *Eut* operon-containing microbes (H, P) along with increased expression of *ARID3a* (I, Q) and miR101a-3p (J, R), reduced expression of *Zo1* (K, S) along with increased gut permeability (FITC-dextran (L, T)), inflammatory markers (*Ilf β* , *Ilf6* and *Tnfa* (M, U)) and impaired MTT (N, V) and ITT (O, W) compared with their normal chow-fed controls. Values presented are the mean of $n=5-8$ mice in each group, and error bars are the SEM. * $p<0.05$, ** $p<0.01$, *** $p<0.001$ are statistically significant analysed by the t-test and/or ANOVA. ANOVA, analysis of variance; CMT, cecal microbiota transplantation; FMT, faecal microbiota transplantation; HFD, high-fat diet; ITT, insulin tolerance test; MTT, meal tolerance test.

(both db/db and DIO) CMTs compared with the lean CMT recipients (figure 7A). Similarly, the expression of *ARID3a* and miR101a-3p was significantly increased, and *Zo1* was decreased predominantly in the ileum of obese CMT recipients as well as of ethanolamine treated mice (figure 7B–G), collectively suggesting that ethanolamine-metabolising bacteria declined primarily in the ileum and was linked with reduced *Zo1* and increased *ARID3a*/miR101a-3p axis.

Further, to identify the cause for the reduction of ethanolamine-metabolising bacteria in obese/diabetic gut, we tested whether certain ethanolamine dominated diets reduce the abundance of these bacteria in gut. Lard in a high-fat diet (HFD) and meat-supplemented diets (MSD) could be a rich source of ethanolamine, and thus could impact gut permeability. Interestingly, 1-week feeding of an HFD (60% calories from fat) and MSD significantly reduced the expression of *Eut* operon in the mouse faeces (figure 7H,P, online supplemental figure 17a,b). Also, 1 week of HFD and MSD fed mice increased the expression of *Arid3a* and miR-101a-3p, and reduced *Zo1* expression in the ileum, increasing gut permeability, inflammation and abnormalities in glucose metabolism (figure 7I–O and Q–W), suggesting that HFD- and MSD reduced the ethanolamine-metabolising bacteria, leading to increased gut permeability, inflammation

and glucose metabolic dysfunctions via increasing ethanolamine/*Arid3a*/miR-101a-3p axis and reducing *Zo1*. Notably, the long-term (5 months) feeding of HFD gradually reduced expression at the *Eut* operon and increased *Arid3a* and miR-101a-3p expression, along with reduced *Zo1* expression and development of leakiness and glucose metabolic dysfunctions in a time-dependent manner (online supplemental figure 18a–h). Overall, these results indicated that ethanolamine-metabolising microbes reduced primarily in ileal section of intestine and linked with increased gut permeability and inflammation, along with impaired *ARID3a*/miR101a-3p/*Zo1* axis and feeding HFD and MSD induced these changes.

Restoring ethanolamine-metabolising capacity in gut microbiota using a human-origin probiotic therapy reduces gut permeability, inflammation and impairment in glucose metabolism

Our results showed that the ethanolamine increase in the obese gut was due to its reduced turnover by microbiota, and such a raised ethanolamine stimulated *ARID3a* binding on miR promoter to elevate miR-101a-3p, which reduced *Zo1* and caused elevated gut permeability. We hypothesised that restoring

microbiome capacity to metabolise ethanolamine can reverse these abnormalities. First, we determined the common gut microbes that express *Eut* operon. Our non-targeted in-silico prediction analyses showed that several commensal bacteria such as *Lactobacilli*, *Bifidobacteria*, *Akkermansia*, *Bacteroides*, *Clostridium*, *Streptococcus* and *Erysipelatoclostridium* express *Eut* operon (online supplemental figure 19a–d and online supplemental table 7). Thus second, we screened an array of novel human-origin strains of *Lactobacillus*, *Bifidobacteria*, *Erysipelatoclostridium*, *Clostridium* and *Streptococcus* for ethanolamine-metabolising ability and found that the *Lactobacillus* (*L.*) *rhamnosus* HL-200 (HL-200) strain exhibited the highest activity in metabolising ethanolamine (figure 8A, upper panel). Also, HL-200 showed the highest expression of *Eut* operon among strains tested (figure 8A, lower panel). Third, 1-week feeding of HL-200 significantly decreased ethanolamine-induced gut permeability, inflammation and impairment in glucose metabolism by increasing *Eut* operon expression, decreasing *ARID3a*, miR-101a-3p, increasing *Zo1* expression and protecting impairment in glucose metabolism (figure 8B–M, online supplemental figure 20a–f). Notably, the feeding of HL-200 also suppressed an increase in gut permeability, endotoxaemia, inflammation and dysfunction in glucose metabolism by suppressing *ARID3a* and miR-101a-3p expression and increasing *Zo1* expression in MSD mice compared with the isocaloric diet-fed control mice (figure 8N–U, online supplemental figure 21a,b). Overall, these results demonstrated that the increased ethanolamine derived from the diet could be reduced by replenishing the ethanolamine-metabolising function of microbiota, using a probiotic HL-200 therapy to reverse ethanolamine-induced and MSD-induced elevation in gut permeability, inflammation and impairment in glucose metabolism characteristics of T2D.

DISCUSSION

Low-grade chronic inflammation is a well-established key driver of obesity-associated impairment in glucose metabolism or risk of T2D.^{25,26} While many sources of inflammation exist, treatable and safe targets are elusive. Multiple emerging lines of evidence point to elevated gut permeability, which allows the release of proinflammatory molecules from the gut to the systemic circulation, as an understudied target of inflammation in patients with obesity and T2D. Abnormalities in microbiota (dysbiosis) co-occur with elevated gut permeability, inflammation and impaired glucose metabolism. However, whether and how obese microbiota might mechanistically contribute to elevated gut permeability and inflammatory syndrome of obesity remain largely unknown. Here, we demonstrated that the transplantation of the intestinal microbiota (both faecal and cecal) from genetic- (db/db) and DIO mouse models to normoglycaemic, lean and conventional mice, significantly increased gut permeability, inflammation and impairment in glucose metabolism in the recipient mice, thus confirming the causal role of such microbiota in instigating gut permeability, inflammation and metabolic dysfunctions such as an increase in body weight gain, food intake and impaired meal tolerance test (MTT) and insulin tolerance test (ITT). The rise in fasting insulin and HOMA-IR of obese microbiota recipient mice indicates that obese microbiota induces pancreatic β -cell dysfunction and insulin resistance. Although hyperglycaemia induces a breakdown of tight junction barriers and elevated gut permeability,²⁷ suggesting that obese microbiota dysbiosis and impairment in glucose metabolism are bidirectional and the exact mechanisms of how microbiota dysbiosis or hyperglycaemia elevates gut permeability remain

elusive. Results here indicated that obese microbiota induced gut permeability to increase inflammation by allowing leakage of proinflammatory LPS/endotoxaemia and impairment in glucose metabolism. These interpretations are based on multiple pieces of evidence that indicate that chronic inflammation accelerates both β -cell dysfunction and insulin resistance^{28,29}; thus, obese microbiota-mediated promotion of inflammation via elevated gut permeability resulting increase flux of endotoxins from gut to blood may be causal for metabolic dysfunction.

To further understand the mechanism by which obese microbiota transplantation induces gut permeability, we demonstrated that obese microbiota reduced the expression of *Zo1*, indicating that they induce gut permeability by dampening gut barrier function by reducing the expression of tight junction proteins- *Zo1*. Gut barriers are complex but well orchestrated, allowing selective permeability of nutrients, water and ions from gut lumen to blood while restricting the translocation of antigens, endotoxins and microbes from gut to blood that can pass across the intestinal epithelium between the cells (paracellular) and/or through cells (transcellular). Increased permeability of low molecular weight (4 kDa) FITC-dextran—a known indicator of paracellular entry, while high molecular weight (40 kDa) FITC-dextran, LPS and 16S rRNA translocation indicate transcellular and paracellular. Here, we saw that obese gut microbiota transplantation induces the permeability of both paracellular and transcellular, with less known mechanisms. Tight junction complexes tie the adjacent cells by establishing connections through their cytoskeletons via scaffolding proteins like *Zo1* and regulate paracellular translocation. Because obese microbiota primarily reduces *Zo1*, their main impact may be to increase paracellular translocation bacteria and proinflammatory bacterial products such as LPS/ endotoxins. However, microbiota in obese gut may also impact their entry through multiple mechanisms like LPS entry through pinocytosis, phagocytosis by goblet and dendritic cells, and others.^{5,30–32} Further comprehensive studies will address how obese microbiota induces paracellular versus transcellular permeability in gut. Notably, the FCM recapitulated the effects of FMT on gut permeability, indicating that FCM can be used as an alternative model to investigate detailed microbiota-mediated mechanisms of paracellular and transcellular permeabilities in future studies. These results also support our previous observations demonstrating that microbiota metabolites are key mediators of microbiota interactions with the host-cells.³³ Therefore, in our next steps using unbiased and non-targeted metabolic approaches, we have discovered a metabolite-ethanolamine, which significantly accumulates in the gut of obese mice and patients and induces gut permeability by reducing the expression of *Zo1* in in vitro, ex vivo and in vivo models.

As a further step to delineate the detailed mechanism involved in obese microbiota and ethanolamine-mediated reduction in *Zo1* expression and elevation in gut permeability, global microRNA expression analyses revealed that the obese microbiota and ethanolamine primarily increase the expression of miR-101a-3p. Further, overexpressing *miR-101a-3p* using lentiviral delivery through enema reduced *Zo1* expression, which in turn induced gut permeability, endotoxaemia and inflammation. Our in silico analyses further discovered that *Zo1* mRNA has miR-101a-3p binding sites; our mRNA stability assay revealed that the ethanolamine-induced miR-101a-3p bound to *Zo1* mRNA and reduced its stability, thus diminishing *Zo1* expression. The miR-101a-3p regulates a myriad of cellular processes in cancer biology and other human diseases^{34–36}; however, our study is to best of our knowledge, the first to unveil its role in regulating gut permeability and sensing microbiota signals through

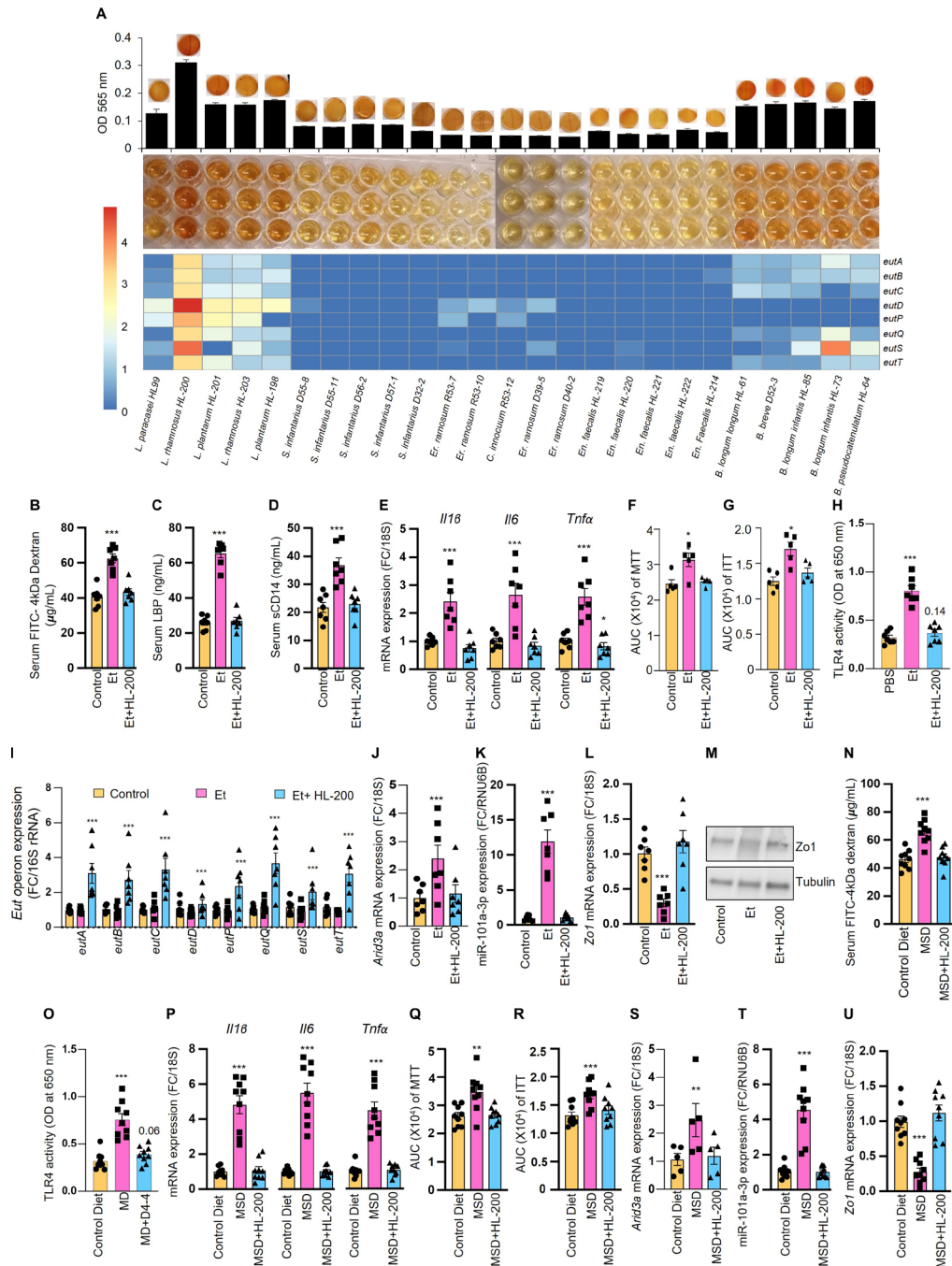


Figure 8 A probiotic therapy restores ethanolamine-metabolising capacity in microbiota which in turn mitigates elevated gut permeability, inflammation and metabolic impairment by restoring homeostasis in ARID3a/miR-101a-3p/Zo1 axis. (A) Screening of ethanolamine-metabolising capacity of human origin probiotics using a colorimetry assay and measuring expression of ethanolamine using operon genes to find *Lactobacillus rhamnosus* HL-200 (HL-200) as a potential ethanolamine-metaboliser. (B–G) Feeding of HL-200 to mice significantly reduced the ethanolamine mediated elevation in gut permeability (FITC-dextran (b), LBP (c) and sCD14 (d)), inflammation (*Il1 β* , *Il6* and *Tnfa*) (e) and impaired area under curve (AUC) MTT (F), AUC ITT (G). (H) The serum of HL-200 fed mice also show less TLR4 activity in HEK-Blue mTLR4 cells treated with serum. (I–M) It also increased the abundance of *Eut* operon expressing microbes (I) and reduced expression of ARID3a (J), and miR-101a-3p (K) and increased *Zo1* (both mRNA and protein) (L,M) compared with controls. (N–U) In addition, HL-200 treatment also significantly reduced the meat supplemented diet (MSD) feeding induced elevation in gut permeability (N), serum-mediated TLR4 activity (O), inflammation (*Il1 β* , *Il6* and *Tnfa*) (p), and impair AUC MTT (Q) and AUC ITT (R) along with reduced ARID3a (S) and miR101a-3p (T) along with increased expression of *Zo-1* mRNA (U) compared with MSD treated controls and restored them close to control diet-fed mice. Values presented are mean ($n=5-8$ mice per group) and error bars as the SE of means. Microbial culture experiments were performed in triplicates and repeated 2–3 times. * $p<0.05$, ** $p<0.01$, *** $p<0.001$ are statistically significant analysed by the t-test and/or ANOVA. ANOVA, analysis of variance; ITT, insulin tolerance test; MSD, meat-supplemented diet; MTT, meal tolerance test.

ethanolamine. Further, an untargeted promoter pulldown chromatin immunoprecipitation assay discovered that the transcription factor-ARID3a³⁷ binds to the miR-101a-3p promoter and increases its expression in response to ethanolamine and/or obese microbiota. These results offer the first evidence that a microbial metabolite-ethanolamine in an obese gut enhanced ARID3a binding on the promoter of miR-101a-3p, which, in turn, destabilised mRNA stability of *Zo1*, resulting in reduced *Zo1* expression and weak intestinal barriers and finally inducing gut permeability. These results create future opportunities to test whether miR-101a-3p inhibitor-based therapy can show efficacy against elevated gut permeability and its associated diseases.

To further understand the reason and mechanisms of increased ethanolamine in the obese gut, we measured the abundance of ethanolamine metabolising bacteria that express ethanolamine operon genes such as *eutA*, *eutB*, *eutC*, *eutD*, *eutP*, *eutS*, *eutT*. We showed that the expression of these genes was significantly reduced in the gut of obese mice, primarily in the small intestine (ileum), indicating the reduced ethanolamine metabolising bacteria in the obese small intestine cause a higher accumulation of ethanolamine, which, in turn, results in increased gut permeability through modulating ARID3a/miR101a-3p/*Zo1* axis. Notably, a significant reduction in the abundance of ethanolamine metabolising bacteria was also observed in obese humans, indicating that this mechanism is a clinically important hallmark of elevated gut permeability and metabolic inflammation in obese patients. In an effort to better understand the process leading to reduced ethanolamine metabolising bacteria in the obese gut, we hypothesised that oversupply of ethanolamine or high calories through diet or other sources reduces the ethanolamine metabolising capacity of the microbiota. Ethanolamine is a common constituent of animal, human and bacterial cells and remains a valuable source of carbon and nitrogen for several bacteria capable of its catabolism.³⁸ Ethanolamine is an ingredient of cell membrane phospholipid phosphatidylethanolamine of host and bacteria produced during the rich turnover of intestinal epithelial cells.³⁸ Thus, increased ethanolamine in the gut could be due to overconsumption of animal products and/or increased intestinal cellular turnover. Notably, we showed that HFD (including lard as an ethanolamine source) and MSD feeding significantly reduced ethanolamine metabolising bacteria in the gut and induced gut permeability, inflammation and impairment in glucose metabolism by reducing *Zo1* via ARID3a/miR101a-3p axis. These results support our first point, that increased ethanolamine supplied through the diet suppresses the ethanolamine metabolising capacity of microbiota. In a previous study, we reported that the gut of obese mice expresses a higher level of cellular turnover genes,³⁹ supporting the idea that increased cellular turnover of gut epithelial cells can be an additional source of extra ethanolamine in gut. Studies to decipher the contribution of diet versus host-cell derived ethanolamine are therefore needed. Overall, these results indicate that the gut microbiota's ability to destroy detrimental metabolites like ethanolamine property reduces the detrimental burden on gut epithelia. Thus, preserving enough ethanolamine-metabolising bacteria can help in maintaining normal intestinal epithelial integrity, permeability and inflammation, which in turn may prevent metabolic dysfunctions.

We used probiotics to increase the reservoir of ethanolamine-metabolising bacteria in the gut, based on our in-silico analysis showing many probiotic genera like *Lactobacillus* and *Bifidobacteria* express *Eut* operon. As probiotics are live bacteria that confer beneficial effects on host health, potentially by modulating gut microbiota,⁴⁰ developing probiotics with

ethanolamine-metabolising function could be clinically applicable to restoring the microbiota's ethanolamine-metabolising property to benefit patients with obesity and T2D. To this end, we screened multiple human-origin probiotics strains such as *Lactobacillus*, *Bifidobacteria*, *Streptococcus*, *Erysipelatoclostridium*, *Clostridium* and *Enterococcus* for their ethanolamine-metabolising capacity and found that *L. rhamnosus* HL-200 was highest ethanolamine metaboliser among them. Notably, HL-200 probiotic therapy reduced the adverse effects of ethanolamine and/or MSD on gut permeability, endotoxaemia, inflammation and metabolic dysfunctions by suppressing ARID3a/ miR101a-3p and preserving the expression of *Zo1*. Although, probiotics have been used for many years, the definitive demonstration of their activity and identification of the mechanisms involved have remained an enormous challenge. Our study support the impact of HL-200 probiotics-based approach for counteracting elevated gut permeability and inflammation by restoring the ethanolamine metabolising capacity of microbiota through defined mechanism of manipulating ARID3a/miR101a-3p/*Zo1* axis. However, whether HL-200 therapy promotes the intrinsic ethanolamine-metabolising bacteria of existing microbiota or enriches the gut microbiota predominantly remains to be explored. Overall, these results suggest that restoring ethanolamine-metabolising capacity in the gut using HL-200 probiotic therapy strengthens intestinal epithelial barrier functions and reduces adverse effects of an unhealthy diet on gut permeability, inflammation and metabolic functions, thus may be helping in reducing the risk of T2D in individuals with obesity and/or maintaining better glucose metabolism.

Overall, our study offers, for the first time, a compelling and comprehensive mechanism to account for the elevated gut permeability and subsequent inflammation and dysfunctions of glucose metabolism observed in patients with obesity. We also show a unique property of gut microbiota to remove the end products such as ethanolamine coming from animal-based diets and dead gut cells, preventing their adverse effects on gut barriers. Our study showed how a decline in ethanolamine-metabolising capacity of microbiota in humans and mice induced elevated gut permeability, inflammation and dysfunctions in glucose metabolism. Finally, this study paves the way for novel strategies to restore such ethanolamine-metabolising capacity of microbiota by using a human-origin probiotic therapy and holding promising translational potential.

METHODS

Animal studies

Donor mice: C57BL/6J (B6) or lean mice and leptin receptor knock-out (db/db) mice were purchased from Jackson Laboratory (Bar Harbor, Maine, USA) and were acclimatised for 2 weeks in our vivarium by maintaining under 12 hours light-dark cycle before the start of experiments or collection of stools. At the age of 4 weeks, the mice (n=5) were divided into four groups- (1) B6-NC (lean) fed with normal chow, (2) B6-LFD-fed with a LFD (10% kcal fat, Research Diets Inc, New Brunswick, USA, NJ), (3) db/db- fed with normal chow and (4) DIO- B6 mice fed with HFD (60% kcal fat, Research Diets, New Brunswick, New Jersey, USA). When mice were 16 weeks old, faecal samples were collected from each group for microbiome, metabolite, FMTs, CMTs and FCM studies. For FMT and CMT studies, B6 mice (age of 8 weeks) were divided into three groups (n=5–8 in each group): (1) lean-FMT/CMT, (2) db/db-FMT/CMT and (3) DIO-FMT/CMT), and, after gut cleansing using antibiotics and polyethylene glycol (as published and described

earlier by us and others^{41–43}) recipient mice were administered lean, db/db and DIO faecal/cecal slurry, respectively, for 7 days. Daily body weight, food and water intake data were collected, and stool collection and gut permeability, MTT, and ITT assays were done during/after treatments. For ethanolamine administration studies, 8–10 week old B6/lean mice (n=5–8 per group) were treated daily with ethanolamine (1 gm/kg body weight) for up to 7 days by oral gavage; data and samples were collected at the indicated time points. For the MSD feeding study, we fed 8–10 weeks-old mice (n=6–9) with MSD compared with an isocaloric control diet (online supplemental table 8a,b) for 2 weeks and collected data and samples. For lentivirus transfection studies in mice, the lentiviral particle carrying mimetic-*miR-101a-3p* was administered through enema twice a week in B6 mice and compared with scrambled miRNA lentivirus ingested controls (n=5 in each group). Healthy B6 mice were anaesthetised with 3.75% isoflurane and were administered with Lentivirus carrying *miR-101a-3p* inhibitor, mimetics or scrambled miRNA sequence through an enema. Mice were given an enema of 100 μ L 50% ethanol (v/v in ddH₂O), and then, after 2 hours, 100 μ L of a vehicle or viral vector solution containing a titre of 0.5×10^8 transducing units (TU) administered intrarectally through a 1.2 mm diameter catheter. The mice were inverted for 30 s after administration of the enema to prevent leakage. After measuring gut permeability, mice were euthanised to collect tissues for further analyses. For probiotic therapy experiments, the B6 mice were also treated with ethanolamine (1 gm/kg body weight) and probiotics *L. rhamnosus* HL-200 (1×10^{11} CFUs/mice/day) or the combination for 7 days and compared with PBS-only administered controls. Also, MSD with or without probiotics HL-200 were fed to B6 mice (n=9/group) for 1 week and compared with control diet-fed controls. All the animal experiments and procedures were approved by the IACUC of Wake Forest School of Medicine and the University of South Florida.

Measurements of body weight, food and water intakes

Body weight was measured daily or weekly using a vivarium-dedicated electronic balance. Food and water intakes were also measured daily by subtracting the amount of food/ water from the leftover amount per day.

Blood glucose, serum insulin and HOMA-IR measurements

Blood glucose was measured using EvenCare ProView Blood Glucose metre (Medline Industries, Illinois, USA). Insulin was measured using ELISA kits (Alpco, New Hampshire, USA). HOMA-IR was calculated using the formula (fasting insulin (μ U/L) \times fasting glucose (nmol/L)/22.55).

MTT and ITT assays

MTT was done in 10 hours fasted mice by administering oral gavage of 200 μ L meal solution/mouse (2 g/kg body weight containing the solution of 570 mg protein (Ensure Original nutrition powder (Abbott) and 30 mg of dextrose in 1.8 mL of cell culture grade PBS) and blood glucose levels were measured using an EvenCare blood glucometer at 0 (before), 15, 30, 60 and 120 min after meal ingestion. For ITT, 4–6 hours fasted mice were given intraperitoneal injections of 0.8 U/kg body weight of insulin (Humulin R, Eli Lilly, Indiana, USA) and blood glucose was measured at 0, 15, 30, 60 and 120 min after insulin administration.

Gut permeability assay in mice

Four hours prefasted mice were orally treated with 1 g/kg body weight FITC-dextran-4kDa, 40 kDa, LPS conjugate (4kDa,

40 kDa and LPS from *Escherichia coli* O55:B5, Sigma, Missouri, USA), and blood was collected after 4 hours to take the readings. Serum was isolated from blood to measure the appearance of FITC fluorescence at 485 nm excitation and 530 nm emission, using 96-well plate reader (POLARstar Omega, BMG Labtech, North Carolina, USA), which was calculated using FITC-dextran standard curve as described by us.⁴²

Gut permeability, endotoxaemia and microbial translocation markers in serum

Systemic gut permeability markers such as LBP (Hycult Biotech, Pennsylvania, USA) and sCD14 (R&D Systems, Minnesota, USA) were measured in serum using ELISA kits. The endotoxin quantity in the systemic circulation using the Pierce Chromogenic Endotoxin Quantitation Kit (Pierce Biotechnology, Illinois, USA), following the manufacturer's instructions. Further, proinflammatory activity of leaked LPS in serum was measured by using the secreted embryonic alkaline phosphate (SEAP) reporter activity in HEK-Blue mTLR4 cells (InvivoGen, California, USA), as described elsewhere.⁴⁴ HEK-Blue mTLR4 cells were cultured in DMEM supplemented media with 10% FBS and selective antibiotics (InvivoGen). HEK-Blue mTLR4 cells were seeded (50 000 cells/well) in 96-well plates in 100 μ L of HEK-Blue detection medium. The HEK-Blue mTLR4 cells were treated with 5% mouse serum and incubated for 24 hours at 37°C, 5% CO₂. SEAP activity, an indicator of TLR4 activity, was analysed based on spectrophotometric absorbance at 650 nm in microplate reader with appropriate standard. In addition, the bacterial DNA in serum was extracted and enriched by using the QIAamp DNA microbiome kit (Qiagen, Maryland, USA) following the manufacturer's instructions. The microbial DNA V3–V4 region was amplified using the Bact-0341F (5'- CCTACGGGNGGCWGCAG-3') and Bact-0805R (5'- GACTACHVGGGTATCTAATCC-3') primers. All the reactions were carried out at least in triplicates.

Microbiota analyses

Genomic DNA was extracted from mouse faeces using the Qiagen DNA Stool Mini Kit (Qiagen), and the V4 region of bacterial 16S rDNA was amplified using primers 515F (barcoded) and 806R.⁴⁵ The amplified DNA was purified and quantified with AMPure magnetic purification beads (Agencourt, Beckman Coulter, California, USA) and Qubit-3 fluorimeter (Thermo Fisher Scientific, Massachusetts, USA), respectively. Equal amounts (8 pM) of the amplicons were applied for sequencing using the Illumina MiSeq sequencer (MiSeq reagent kit V3, Illumina, California, USA). The sequences were demultiplexed, quality filtered, clustered and analysed with the Quantitative Insights into Microbial Ecology and R-based analytical tools as we published earlier.^{42 45–47}

Metabolomics analysis

Global metabolomics was performed using NMR spectrometry in the faecal samples, using a method described by Gratton *et al.*⁴⁸ with slight changes. The extracted aqueous samples were mixed with phosphate buffer containing 10% D₂O and 0.1 mM trimethylsilyl propionate (TSP). NMR experiments were carried out on a Bruker Ascend 400 MHz high-resolution NMR (Bruker Biospin, Ettlingen, Germany) using a 1D first increment of a NOESY (noesygppr1d) with water suppression and a 4 s recycle delay. All NMR spectra were phased and referenced to TSP in TopSpin V.4.06 (Bruker BioSpin, Ettlingen, Germany). The NMR spectra were analysed in Amix V.4.02, and a manual pattern

was created using the metabolites peaks range determined by Chenomx V8.4 (Chenomx, Edmonton, Alberta, Canada) to extract the metabolite peak intensities. Total intensity normalisation was applied before further data analysis.

Ethanolamine operon quantification

Genomic DNA was extracted from faeces and bacterial cells using the Qiagen DNA Stool Mini Kit (Qiagen). After normalising an equal amount of DNA, the qRT-PCR analyses were performed using PowerUp SYBR Green master mix (ThermoFisher Scientific) and ethanolamine-metabolising operon genes (online supplemental table 9). The gene expression was calculated using the $\Delta\Delta$ CT method while normalised with 16S rRNA as an internal control.

Enteroids development and treatments

To develop mouse enteroids, the entire small intestine was collected from mice and flushed with precooled Dulbecco's phosphate-buffered saline (DPBS, Lonza, Maryland, USA). The lengthwise cut-opened ileum was washed with cooled PBS and fragmented into 2 mm pieces, then transferred to a 50 mL conical flask containing cleaned precooled PBS. Tissue fragments were incubated in 25 mL of prewarmed Trypsin (Gibco, New York, USA) on a rocking platform for 15 min. After removing the trypsin, tissue pieces were washed with 10 mL precold PBS with 0.1% bovine serum albumin (BSA from Fisher Scientific) and filtered in a 50 mL conical tube through a 70 μ m cell strainer (Corning, North Carolina, USA). These pieces were then centrifuged at $290 \times g$ for 5 min at 4°C. The intestinal crypt-containing pellets were suspended in the 10 mL cold DMEM: F-12 (Gibco) and centrifuged at $500 \times g$ for 10 min, followed by resuspending in 150 μ L IntestiCult Organoid Growth Medium (StemCell Technology, Canada) with 50 μ g/mL gentamicin (Gibco). The Matrigel Matrix (Thermo Fisher Scientific) was added to the suspension, and the mixture of 50 μ L was used to form a dome at the centre of a prewarmed 24-well culture plate and incubated at 37°C and 5% CO₂ for 30 min to allow the Matrigel to set. To maintain the cultures, the IntestiCult Organoid Growth Medium was changed three times per week. On day 10, the enteroids were treated with faecal condition media (FCM), metabolites and ethanolamine, with three replicates in each group. The enteroids were harvested after 2 days of treatment(s) for miRNA, mRNA and protein analyses. Experiments were repeated 2–3 times.

FCM preparation

Fresh faeces collected from mice were snap-frozen in liquid nitrogen and crushed using a mortar and pestle. The finely powdered faeces (100 mg) were suspended in 100 mL cold DMEM (Gibco) media and kept on a shaker at a speed of 200 rpm for 1 hour to mix properly in a cold room. The suspended media was filtered twice through 0.45 μ m filters (Corning), and twice again through 0.22 μ m sterile syringe filters in sterile conditions. The 1:40 diluted FCM was used to treat the intestinal enteroids and cells.

TEER assay in Caco-2 cell monolayers

Human intestinal epithelial Caco-2 cells (ATCC, Virginia, USA) were seeded in 12-well transwell plates containing an apical chamber made of polyester membrane filters with 0.4 μ m pore size (Corning) at a density of 3×10^5 /well. The culture medium from both the apical and basolateral compartments was changed every 2 days. The cells are allowed to fully differentiate for 21 days, and fully differentiated cells with no leakage tested were

challenged with FCM and metabolites for the next 8 hours with continuous measuring of TEER values, using an EVOM² Epithelial Voltmeter (WPI, Florida, USA). The blank inert resistance value (the insert with only culture media) was subtracted from the measured resistance value of each sample, and the final resistance in $\text{ohm} \times \text{cm}^2$ was calculated by multiplying the sample resistance by the area of the membrane.

FITC-dextran permeability assay in Caco-2 cell monolayers

Fully differentiated Caco-2 cells up to 21 days, the FITC-dextran 4 (4 kDa; Sigma) solution (1 mg/mL) was added to the apical (upper) side of the monolayers along with treatments of corresponding FCM and metabolites. The basolateral side media was collected to determine the FITC levels using the fluorescent reader and standard curve.⁴²

Western blots

Total proteins from tissues, enteroids and cells were extracted using homogenised lysis buffer, as mentioned in our previous publications.⁴² Proteins were resolved by SDS-PAGE electrophoresis and transferred to the PVDF membrane for Western blotting. Membranes were developed with primary antibodies zona occludins-1 (Zo1), Invitrogen) and Arid3a (Santa Cruz Biotechnology, Texas, USA), followed by secondary antibodies and developed with a chemiluminescent kit (ECL, Thermo Scientific) and imaged on PXi with the GeneSys software (SynGene, Maryland, USA). Tubulin was used as the internal loading control.

RNA isolation and gene expression analyses

Total and small RNAs were isolated from tissue, enteroids and cells collected and stored in RNAlater solution (Ambion, ThermoFisher) at -80°C using RNeasy Mini Kit (Qiagen). Total RNA from bacterial cells were extracted using RNeasy Protect Bacteria reagent and RNeasy Mini Kit (Qiagen). The complementary DNA (cDNA) was synthesised from total and small RNAs using High-Capacity cDNA reverse transcription kit (Thermo Fisher Scientific). The normalised cDNA of each sample was used to run the qRT-PCR using a 7900 real-time PCR machine (Thermo Fisher Scientific) using SYBR Green master mix (Thermo Fisher Scientific) and gene-specific primers (online supplemental tables 1 and 10). The relative gene expression rate was analysed using $\Delta\Delta$ CT method normalised by 18S as an internal control. All the reactions were performed at least in triplicates.

miRNA profiling and expression analyses

For miRNA profiling, the total small RNA was extracted from enteroids treated with FCMs of B6, db/db, and DIO, using miRNeasy Mini kit (Qiagen) and analysed by the NanoString nCounter miRNA Assays, using 50–100 ng of total RNA from each sample in four replicates, and using eight positive control probes and eight negative control probes. Data were analysed using nSolver analysis software V4.0. Each miRNA background correction count was carried out by subtracting mean + 2 SD of eight negative control probes as a cut-off. The miRNA of count 50 or more after background correction was further used for analysis. The individual miRNA expression was quantified, using qRT-PCR by converting small RNAs to cDNA using TaqMan miRNA Reverse Transcription kit (ThermoFisher) and TaqMan 2X Universal PCR Master Mix, No AmpErase UNG (ThermoFisher) on 7900 real-time PCR machine. The TaqMan primers were used for specific miRNAs, and RNU6B was used as an internal control as mentioned in online supplemental table 11; and relative expression was calculated using $\Delta\Delta$ CT method.

miRNA transfection to Caco-2 cells

Caco-2 cells were grown up to 80%–90% confluency and were transfected with miRIDIAN mimetic negative control #1, miRIDIAN mimetic mmu-miR-101a-3p and miRIDIAN hairpin inhibitor mmu-miR-101a-3p (Horizon Discovery, Pennsylvania, USA) as mentioned in online supplemental table 11, using Lipofectamine 3000 transfection kit (ThermoFisher). The cells were harvested after 48 hours for miRNA, mRNA and protein expression analyses.

Zo1-over-expression in Caco-2 cells

Caco-2 cells were grown up to 80%–90% confluency and were transfected with precision lentiORF RFP positive control viral particles and precision lentiORF TJP1 w/Stop codon viral particles as mentioned in online supplemental table 11 using DharmaFECT kb DNA transfection reagent kit (Horizon Discovery) and subjected for TEER and FITC-dextran assay. The cells were harvested after 48 hours for *Zo1* mRNA expression analyses.

Promoter luciferase assay

Caco-2 cells seeded in a 96-well plate at a density of 2×10^4 cells/well were transfected with *miR-101a-3p* promoter pMK-RQ (KanR) reporter vector of 4 different nucleotide sequence (–1 to –500, –1 to –1000, –1 to –1500 and –1 to –2000 bps) from its TSS (transcription start site) and pMK-RQ (control vector) using Lipofectamine 3000 transfection kit (ThermoFisher) as mentioned in online supplemental table 11. The TSS of *miR-101a-3p* is located at position: chr1 65067704 (genome version hg38) as reported earlier.⁴⁹ The cells were collected at various time points (0, 1, 3, 5, 7 and 10 hours) after transfection. The expression level of firefly luciferase reporter gene was measured using Pierce Firefly Luciferase Glow Assay kit.

mRNA stability assay

Caco-2 cells were transfected with mimetic miR-101a-3p and inhibitor miR-101a-3p, and cDNA was synthesised after harvesting the transfected cells at 0, 1, 3, 6, 12, 24 and 48 hours time points. The half-life of the *Zo1* mRNA expression was calculated using a formula: $E(t) = E_0 \times (1/2)^{(t/t_{1/2})}$, where 'E(t)' stands for expression of *Zo1* at time point 't' after transfection with mimetic miR-101a-3p and inhibitor miR-101a-3p, 'E₀' stands for the initial expression level of *Zo1* before transfection, 't' stands for the time elapsed after transfection, 't_{1/2}' stands for the half-life in the *Zo1* expression on transfection with mimetic miR-101a-3p and inhibitor miR-101a-3p.

Chromatin immunoprecipitation protein-DNA pulldown assay

Fully differentiated 21-day old Caco-2 cells were treated with 10 μM ethanolamine for 48 hours, and then washed with PBS buffer containing inhibitors (PBSI)- 0.5 mM PMSF (Phenylmethylsulphonyl fluoride), 1 mM sodium vanadate, 0.5 mM Dithiothreitol, 1 μg/mL Leupeptin, 25 mM β-glycerophosphate, 10 mM sodium fluoride, then were harvested and suspended in two package cell volume of buffer A with inhibitors (10 mM 4-(2-hydroxyethyl)-1-piperazineethanesulfonic acid, 1.5 mM magnesium chloride, 10 mM potassium chloride, 300 mM sucrose, 0.5% NP-40) and kept on ice for 10 min. Cells were pelleted by centrifuging at 2600 g for 30 s and resuspended in 2/3 package cell volume with buffer B containing inhibitors (20 mM HEPES, pH 7.9, 1.5 MgCl₂, 420 mM sodium chloride, 0.2 mM EDTA, 2.5% glycerol). After sonication and centrifugation at 10400 g for 5 min, the supernatant was isovolumetrically diluted with buffer D-containing inhibitors (20 mM HEPES, pH 7.9, 100 mM

potassium chloride, 0.2 mM EDTA, 8% glycerol). Total protein (400 μg) of nuclear extract was normalised among the samples, and two drops (40 μL) of streptavidin-agarose bead were suspended, and 4 μg of 5'-biotinylated-*pmiR-101a-3p* (–1000 to –500 bp promoter sequence of *miR-101a-3p* and scrambled sequence as control as mentioned in online supplemental table 11) in 500 μL of PBSI. After rocking this mixture for 2 hours and centrifuging at 550 g for 1 min, the pellet was washed with PBSI for three times and was resuspended in 40 μL of 2X Laemmli sample buffer and incubated for 95°C for 5 min to obtain beads.

Beads were placed onto the polyethylene filter in the Pierce 0.8 mL Centrifuge Columns (Thermo Scientific) and were washed three times by adding 200 μL of washing buffer (50 mM ammonium bicarbonate solution) and centrifugation at 1000 × g for 1 min for each time. The bottom end of the column was capped, and 200 μL of washing buffer containing 10 mM dithiothreitol solution was added. With the top capped, the column was agitated on a tube rotator for 1 hour at 37°C. The bottom cap was removed, and the tube was centrifuged at 1000 × g for 1 min to remove the supernatant. Beads were then incubated in 200 μL of 30 mM iodoacetamide solution for 45 min at room temperature in the dark. Beads were washed with 200 μL of washing buffer three times; further, 200 μL of digestion buffer (50 mM ammonium bicarbonate solution) was added, and the tube was incubated overnight at 37°C. The enzyme reaction was quenched by adding 10 μL of 20% formic acid, and the column was centrifuged to collect flow-through in the collection tube. Beads were washed with 100 μL of 50% acetonitrile containing 0.1% formic acid twice, and the flow-through was combined with the initial eluent. Beads were washed again with 80% acetonitrile containing 0.1% formic acid, and flow-through was collected in the same tube. The solution was dried under vacuum and then prepared in 5% acetonitrile with 1% formic acid and was injected in an liquid chromatography and tandem mass-spectrometry (LC-MS/MS) system consisting of an Orbitrap Velos Pro Mass Spectrometer (Thermo Scientific) and a Dionex Ultimate-3000 nano-UPLC system (Thermo Scientific). Peptides were separated on an Acclaim PepMap 100 (C18, 5 μm, 100 Å, 100 μm × 2 cm) trap column and an Acclaim PepMap RSLC (C18, 2 μm, 100 Å, 75 μm × 50 cm) analytical column employing a linear gradient consisting of water with 0.1% formic acid (A) and acetonitrile with 0.1% formic acid (B) where the gradient was from 5% B at 0 min to 40% B at 105 min. MS spectra were acquired by data-dependent scans consisting of MS/MS scans of the ten most intense ions from the full MS scan with a dynamic exclusion option, which was 30 s. To identify proteins, spectra were searched against the UniProt human protein FASTA database (20258 annotated entries, Feb 2018), using the Sequest HT search engine with the Proteome Discoverer V.2.2 (Thermo Scientific). Search parameters were as follows: (1) FT-trap instrument; parent mass error tolerance, 10 ppm; fragment mass error tolerance, 0.6 Da (monoisotopic); enzyme, trypsin (full); number maximum missed cleavages and (2) variable modifications, +15.995 Da (oxidation) on methionine; static modification, +57.021 Da (carbamidomethyl) on cysteine.

Bacterial ethanolamine metabolism screening

We screened 25 human-origin probiotics (5 *Lactobacilli*, 5 *Streptococci*, 9 *Erysipelatoclostridia*, 1 *Clostridium*, 5 *Enterococci* and 5 *Bifidobacteria*) strains for their ethanolamine-metabolising capabilities. These strains were characterised for their genetic identity by DNA sequencing and general safety profiles like devoid of a pathogenic island in the genome and

antibiotic-resistant properties along with probiotic attributes such as antibacterial activities, bile acid tolerance and epithelial cell adhesion as published earlier.⁵⁰ Bacterial streaks were grown for 48 hours in the MRS agar media plates containing 10 mM ethanolamine. Then plates were overlaid with 5 mL 500 mM ethanolamine MRS agar and incubated at 37°C for 1 hour, followed by adding 5 mL of 2,4-dinitrophenylhydrazine in each plate and further incubating for 3 min. Then the solution was discarded, and 5 mL of 5 M potassium hydroxide was added. Pink to purple zones were developed around the bacterial streaks, demonstrating the conversion of ethanolamine to acetaldehyde was quantified. The *L. rhamnosus* HL-200 (HL-200) probiotic was freshly cultured, counted and equal numbers (10⁹ cfu/mL) administered to ethanolamine and MSD-fed mice.

Human samples

The obese stool samples were obtained from Valued Epigenetics Glycaemic Improvements through Weight Loss study (ClinicalTrials.gov Identifier: NCT02869659), and normal weight control stool samples were acquired from Mediterranean Diet and the Gut Microbiome (ClinicalTrials.gov Identifier: NCT03269032). Stool samples were collected, processed and stored with the same protocol and kits from Dr. Yadav's lab.

Statistical analyses

Different datasets were analysed by Student's t-test and one/two-way analysis of variance. Alpha-diversity indices and bacterial abundance between the two groups were compared using an unpaired two-tailed t-test. Hierarchical clustering and heat-maps based on average linkage on Euclidean distance, depicting the patterns of abundance and log values were constructed within R V.6.0, using the 'heatmap.2', 'pheatmap' and 'ggplots' packages. RFA and principal component analysis (PCA) were analysed in R programming V.6.0 using packages 'randomForest', 'ggplot2', 'caret', 'psych', 'ggbplots', 'nnet' and 'devtools'. PCA was applied using all features of the NMR spectra with a PLS-tool box (Eigenvector Research) in Matlab (MathWorks). Welch t-test was applied for statistical significance analysis for metabolites in Amix V.3.9 (Bruker Biospin), and a false discovery rate were applied to control the family wise error. The heatmaps, Volcano Plot, Pathway analysis for pathways and dendrogram were carried out in MetaboAnalyst V.3.0. Unless otherwise stated, all the values presented here are means ± SEM. A p < 0.05 was considered statistically significant.

Author affiliations

¹Neurosurgery and Brain Repair, University of South Florida College of Medicine, Tampa, Florida, USA

²USF Center for Microbiome Research, Microbiomes Institutes, University of South Florida Morsani College of Medicine, Tampa, Florida, USA

³Department of Biomedical and Chemical Engineering and Sciences, Florida Institute of Technology, Melbourne, Florida, USA

⁴Department of Internal Medicine, Wake Forest University School of Medicine, Winston-Salem, North Carolina, USA

⁵Wake Forest School of Medicine, Winston-Salem, North Carolina, USA

⁶Department of Animal Genetics and Breeding, West Bengal University of Animal & Fishery Sciences, Kolkata, West Bengal, India

⁷Department of Internal Medicine, University of South Florida College of Medicine, Tampa, Florida, USA

Acknowledgements All the authors are grateful to all the fellow staff and laboratory members of Yadav's lab for their cooperation and help during the study. Special thanks to Jingyun Lee for performing proteomics analysis in Dr. Cristina Furdul's lab; staff of Drs. Jingzhong Ding, Rejeski and Kitzman lab for procuring human samples. We appreciate the help of the diet formulating team in the non-human primate centre at the Wake Forest School of Medicine. We apologise for many

of our colleagues for not being able to be included in citations due to journal's policy restricting total citations ~50.

Contributors SPM: performed experiments and compiled data; BW: performed global metabolomics and data analyses; JD and JR: provided human samples; CMF: performed proteomics analyses; SJ: contributed significantly to data interpretations, writing manuscripts and intellectual discussions; DK, ST, CB and AK: contributed for intellectual data interpretation, discussion and feedback in manuscript; HY: conceived the idea, secured funding and arranged resources, supervised the study, helped in data interpretations, developed and written manuscript, revised drafts of manuscripts; supervised overall project and will serve the contact person for any further queries. All authors reviewed and approved the final version of the manuscript.

Funding We are thankful for the support provided by National Institutes of Health (NIH) grants R56AG064075, R56AG069676, R21AG072379, RF1AG071762, U01AG076928 and the Department of Defense funding W81XWH-19-1-0236 (for HY), as well as funds and services provided from the Wake Forest School of Medicine, USF Center for Microbiome Research, Microbiomes Institute, and Department of Neurosurgery and Brain Repair, University of South Florida.

Competing interests The intellectual property for HL-200 probiotics is under-review with institutional patent and technology office. HY is a chief scientific officer of the Postbiotics, which has no influence and contribution with the work done in current manuscript.

Patient and public involvement Patients and/or the public were not involved in the design, or conduct, or reporting, or dissemination plans of this research.

Patient consent for publication Consent obtained directly from patient(s).

Ethics approval These studies were approved by Wake Forest School of Medicine Institutional Board and under the ClinicalTrials.gov Identifier: NCT02869659 and ClinicalTrials.gov Identifier: NCT03269032. Participants gave informed consent to participate in the study before taking part.

Provenance and peer review Not commissioned; externally peer reviewed.

Data availability statement Data are available on reasonable request. All data relevant to the study are included in the article or uploaded as online supplemental information. Source data file is uploaded in online supplemental materials.

Supplemental material This content has been supplied by the author(s). It has not been vetted by BMJ Publishing Group Limited (BMJ) and may not have been peer-reviewed. Any opinions or recommendations discussed are solely those of the author(s) and are not endorsed by BMJ. BMJ disclaims all liability and responsibility arising from any reliance placed on the content. Where the content includes any translated material, BMJ does not warrant the accuracy and reliability of the translations (including but not limited to local regulations, clinical guidelines, terminology, drug names and drug dosages), and is not responsible for any error and/or omissions arising from translation and adaptation or otherwise.

Open access This is an open access article distributed in accordance with the Creative Commons Attribution Non Commercial (CC BY-NC 4.0) license, which permits others to distribute, remix, adapt, build upon this work non-commercially, and license their derivative works on different terms, provided the original work is properly cited, appropriate credit is given, any changes made indicated, and the use is non-commercial. See: <http://creativecommons.org/licenses/by-nc/4.0/>.

ORCID iDs

Sidharth P Mishra <http://orcid.org/0000-0001-7586-846X>

Hariom Yadav <http://orcid.org/0000-0003-4504-1597>

REFERENCES

- 1 Donath MY, Shoelson SE. Type 2 diabetes as an inflammatory disease. *Nat Rev Immunol* 2011;11:98–107.
- 2 Gregg EW, Sattar N, Ali MK. The changing face of diabetes complications. *Lancet Diabetes Endocrinol* 2016;4:537–47.
- 3 Cani PD, Amar J, Iglesias MA, et al. Metabolic endotoxemia initiates obesity and insulin resistance. *Diabetes* 2007;56:1761–72.
- 4 Buford TW. (Dis)trust your gut: the gut microbiome in age-related inflammation, health, and disease. *Microbiome* 2017;5:80.
- 5 Burcelin R. Gut microbiota and immune crosstalk in metabolic disease. *Mol Metab* 2016;5:771–81.
- 6 Shemtov SJ, Emami R, Bielska O, et al. The intestinal immune system and gut barrier function in obesity and ageing. *FEBS J* 2022. 10.1111/febs.16558 [Epub ahead of print 21 Jun 2022].
- 7 Ménard S, Cerf-Bensussan N, Heyman M. Multiple facets of intestinal permeability and epithelial handling of dietary antigens. *Mucosal Immunol* 2010;3:247–59.
- 8 Turnbaugh PJ, Ley RE, Mahowald MA, et al. An obesity-associated gut microbiome with increased capacity for energy harvest. *Nature* 2006;444:1027–31.

- 9 Singh R, Chandrashekarappa S, Bodduluri SR, *et al.* Enhancement of the gut barrier integrity by a microbial metabolite through the Nrf2 pathway. *Nat Commun* 2019;10:89.
- 10 Umeda K, Matsui T, Nakayama M, *et al.* Establishment and characterization of cultured epithelial cells lacking expression of ZO-1. *J Biol Chem* 2004;279:44785–94.
- 11 McNeil E, Capaldo CT, Macara IG. Zonula occludens-1 function in the assembly of tight junctions in Madin-Darby canine kidney epithelial cells. *Mol Biol Cell* 2006;17:1922–32.
- 12 Li C, Gao M, Zhang W, *et al.* Zonulin regulates intestinal permeability and facilitates enteric bacteria permeation in coronary artery disease. *Sci Rep* 2016;6:29142.
- 13 Mathewson ND, Jenq R, Mathew AV, *et al.* Corrigendum: gut microbiome-derived metabolites modulate intestinal epithelial cell damage and mitigate graft-versus-host disease. *Nat Immunol* 2016;17:1235.
- 14 Feng YH, Wang Y, Wang P, *et al.* Short-chain fatty acids manifest stimulative and protective effects on intestinal barrier function through the inhibition of NLRP3 inflammasome and autophagy. *Cell Physiol Biochem* 2018;49:190–205.
- 15 Beaumont M, Paës C, Mussard E, *et al.* Gut microbiota derived metabolites contribute to intestinal barrier maturation at the suckling-to-weaning transition. *Gut Microbes* 2020;11:1268–86.
- 16 Ondee T, Pongpirul K, Visitchanakun P, *et al.* Lactobacillus acidophilus LA5 improves saturated fat-induced obesity mouse model through the enhanced intestinal akkermansia muciniphila. *Sci Rep* 2021;11:6367.
- 17 Ghosh S, Whitley CS, Haribabu B, *et al.* Regulation of intestinal barrier function by microbial metabolites. *Cell Mol Gastroenterol Hepatol* 2021;11:1463–82.
- 18 Kumari A, Bhawal S, Kapila S, *et al.* Health-promoting role of dietary bioactive compounds through epigenetic modulations: a novel prophylactic and therapeutic approach. *Crit Rev Food Sci Nutr* 2022;62:619–39.
- 19 Liu S, da Cunha AP, Rezende RM, *et al.* The host shapes the gut microbiota via fecal microma. *Cell Host Microbe* 2016;19:32–43.
- 20 Li MH, Chen WD, Wang YD. The roles of the gut microbiota-mirna interaction in the host pathophysiology. *Mol Med* 2020;26:101.
- 21 Agbu P, Carthew RW. MicroRNA-mediated regulation of glucose and lipid metabolism. *Nat Rev Mol Cell Biol* 2021;22:425–38.
- 22 Tilg H, Zmora N, Adolph TE, *et al.* The intestinal microbiota fuelling metabolic inflammation. *Nat Rev Immunol* 2020;20:40–54.
- 23 Nagpal R, Mishra SP, Yadav H. Unique gut microbiome signatures depict diet-versus genetically induced obesity in mice. *Int J Mol Sci* 2020;21:3434.
- 24 Huang C, Xiao X, Yang Y, *et al.* Correction: microRNA-101 attenuates pulmonary fibrosis by inhibiting fibroblast proliferation and activation. *J Biol Chem* 2019;294:6694.
- 25 Monlun M, Rigalleau V, Blanco L, *et al.* Chronic low grade inflammation in type 2 diabetes—activation of the inflammasomes by circulating metabolites. *Diabetes* 2018;67:1726-P.
- 26 Scheithauer TPM, Rampanelli E, Nieuwdorp M, *et al.* Gut microbiota as a trigger for metabolic inflammation in obesity and type 2 diabetes. *Front Immunol* 2020;11:571731.
- 27 Thaiss CA, Levy M, Grosheva I, *et al.* Hyperglycemia drives intestinal barrier dysfunction and risk for enteric infection. *Science* 2018;359:1376–83.
- 28 Eguchi K, Nagai R. Islet inflammation in type 2 diabetes and physiology. *J Clin Invest* 2017;127:14–23.
- 29 Shoelson SE, Lee J, Goldfine AB. Inflammation and insulin resistance. *J Clin Invest* 2006;116:1793–801.
- 30 Wiest R, Rath HC. Bacterial translocation in the gut. *Best Practice & Research Clinical Gastroenterology* 2003;17:397–425.
- 31 McKay DM, Baird AW. Cytokine regulation of epithelial permeability and ion transport. *Gut* 1999;44:283–9.
- 32 Schoultz I, Keita ÅV. The intestinal barrier and current techniques for the assessment of gut permeability. *Cells* 2020;9:1909.
- 33 Yadav H. Gut microbiome derived metabolites to regulate energy homeostasis: how microbiome talks to host. *Metabolomics* 2016;6:e150.
- 34 Wang C-Z, Deng F, Li H, *et al.* Mir-101: a potential therapeutic target of cancers. *Am J Transl Res* 2018;10:3310–21.
- 35 Hackl M, Brunner S, Fortschegger K, *et al.* Mir-17, mir-19b, mir-20a, and miR-106a are down-regulated in human aging. *Aging Cell* 2010;9:291–6.
- 36 Lippi G, Fernandes CC, Ewell LA, *et al.* MicroRNA-101 regulates multiple developmental programs to constrain excitation in adult neural networks. *Neuron* 2016;92:1337–51.
- 37 Ratliff ML, Garton J, James JA, *et al.* ARID3a expression in human hematopoietic stem cells is associated with distinct gene patterns in aged individuals. *Immun Ageing* 2020;17:24.
- 38 Patel D, Witt SN. Ethanolamine and phosphatidylethanolamine: partners in health and disease. *Oxid Med Cell Longev* 2017;2017:4829180.
- 39 Nagpal R, Newman TM, Wang S, *et al.* Obesity-linked gut microbiome dysbiosis associated with derangements in gut permeability and intestinal cellular homeostasis independent of diet. *J Diabetes Res* 2018;2018:3462092.
- 40 Martin R, Langella P. Emerging health concepts in the probiotics field: streamlining the definitions. *Front Microbiol* 2019;10:1047.
- 41 Ahmadi S, Razazan A, Nagpal R, *et al.* Metformin reduces aging-related leaky gut and improves cognitive function by beneficially modulating gut microbiome/goblet cell/mucin axis. *J Gerontol A Biol Sci Med Sci* 2020;75:e9–21.
- 42 Ahmadi S, Wang S, Nagpal R, *et al.* A human-origin probiotic cocktail ameliorates aging-related leaky gut and inflammation via modulating the microbiota/taurine/tight junction axis. *JCI Insight* 2020;5:e132055.
- 43 Wang S, Ahmadi S, Nagpal R, *et al.* Lipoteichoic acid from the cell wall of a heat killed Lactobacillus paracasei D3-5 ameliorates aging-related leaky gut, inflammation and improves physical and cognitive functions: from C. Elegans to mice. *Geroscience* 2020;42:333–52.
- 44 Anhê FF, Barra NG, Cavallari JF, *et al.* Metabolic endotoxemia is dictated by the type of lipopolysaccharide. *Cell Rep* 2021;36:109691.
- 45 Caporaso JG, Kuczynski J, Stombaugh J, *et al.* QIIME allows analysis of high-throughput community sequencing data. *Nat Methods* 2010;7:335–6.
- 46 Nagpal R, Neth BJ, Wang S, *et al.* Gut microbiome and its interaction with diet, gut bacteria and alzheimer's disease markers in subjects with mild cognitive impairment: a pilot study. *EBioMedicine* 2020;59:102950.
- 47 Nagpal R, Neth BJ, Wang S, *et al.* Modified mediterranean-ketogenic diet modulates gut microbiome and short-chain fatty acids in association with alzheimer's disease markers in subjects with mild cognitive impairment. *EBioMedicine* 2019;47:529–42.
- 48 Gratton J, Phetcharaburanin J, Mullish BH, *et al.* Optimized sample handling strategy for metabolic profiling of human feces. *Anal Chem* 2016;88:4661–8.
- 49 Huang C, Xiao X, Yang Y, *et al.* MicroRNA-101 attenuates pulmonary fibrosis by inhibiting fibroblast proliferation and activation. *J Biol Chem* 2017;292:16420–39.
- 50 Nagpal R, Wang S, Ahmadi S, *et al.* Human-origin probiotic cocktail increases short-chain fatty acid production via modulation of mice and human gut microbiome. *Sci Rep* 2018;8:12649.